AN ABSTRACT OF THE THESIS OF

JAMES ROBERT CARLSON for the DOCTOR OF PHILOSOPHY
(Name of student) (Degree)

in Physics presented on May 14, 1970
(Major) (Date)

Title: $k^- + p \rightarrow k^0 + \Xi^0$ DIFFERENTIAL CROSS SECTION MEASUREMENT AT 1.8 GeV/c

Abstract approved: Redacted for privacy
Howard F. Davis

The differential cross section for the reaction

$$k^- + p \rightarrow k^0 + \Xi^0$$

was measured in a spark chamber experiment for an incident k^- momentum of 1.8 GeV/c. The target was liquid hydrogen confronted by an anti-coincidence counter to insure neutral particle production. A 60 element hodoscope signalled the presence of four charged particles in the final state. The angular distribution of the k^0 in the center of mass for 59 events has been fit to a series of Legendre polynomials and a good fit was obtained using a maximum order of three. An examination of the fitted data reveals a peak in the backward direction, a dip in the forward direction, and some evidence for direct channel resonances.

$K^- + p \rightarrow K^0 + \Xi^0$
Differential Cross Section Measurement at 1.8 GeV/c

by

James Robert Carlson

A THESIS

submitted to

Oregon State University

in partial fulfillment of
the requirements for the
degree of

Doctor of Philosophy

June 1971

APPROVED:

Redacted for privacy

Associate Professor of Physics
in charge of major

Redacted for privacy

Chairman of Department of Physics

Redacted for privacy

Dean of Graduate School

Date thesis is presented May 14, 1970

Typed by Opal Grossnicklaus for James Robert Carlson

ACKNOWLEDGMENTS

I wish to acknowledge the contribution of my advisor, Dr. Howard F. Davis, to the completion of this thesis. My interest in high energy physics sprang from his encouragement, and the succeeding years of research were made possible only by his continuing guidance and inspiration.

During the experiment and subsequent analysis I received considerable advice and knowledge from my fellow graduate student, Del Jauch. Thanks are also due to Dr. Norman Sossong and Dr. Robert Ellsworth who made essential contributions to the construction and operation of the experiment. The assistance of Albert Jaske and Eugene Dunn as well as the Bevatron personnel and other Lawrence Radiation Laboratory groups is greatly appreciated.

TABLE OF CONTENTS

LIST OF FIGURES

LIST OF TABLES

$k^- + p \rightarrow k^0 + \Xi^0$ DIFFERENTIAL CROSS SECTION MEASUREMENT AT 1.8 GeV/C

INTRODUCTION

Since the advent of high energy particle accelerators in the early 1950's, one of the basic tasks of physicists concerned with high energy phenomena has been to classify the so-called elementary particles resulting from baryon[1]-baryon and meson[2]-baryon collisions. The hope is that by ordering these particles according to their properties, certain regularities might show up that would lead to a discovery of the forces involved in their production and decay. A knowledge of the forces is, of course, basic to an understanding of the fundamental structure of matter. The discovery of new particles, however, has proceeded at such a rapid pace that many of the properties of these particles have yet to be accurately determined. Nevertheless, classification schemes have been devised, with one of the most successful being based on unitary symmetry.

In 1961 Gell-Mann (34) and Ne'eman (56) proposed that particles be organized into multiplets derived from the rotation proterties of the group SU(3). Under this system the proton and neutron would be

---

[1] The class of particles containing the proton and those particles whose decay leads to a proton.

[2] The unstable particles which strongly interact with the baryons but whose total number is not conserved.

grouped together with some other particles into an octet of baryons all having a spin of one-half and even parity. Figure 1 shows the positions of these particles in a plot of Y vs T3, where T3 is the third component of isospin and Y is the hypercharge quantum number. Those successes of this classification scheme which led to its general acceptance will not be discussed here since details may be found in several of the references (30, 31, 44).

The neutral cascade particle (Ξ^0) was discovered among cosmic rays (5) and was first observed in an accelerator experiment in 1958 (3). The name is descriptive of its characteristic two-step decay:

$$\Xi^0 \rightarrow \Lambda + \pi^0$$

$$\Lambda \rightarrow p + \pi^-.$$

The mass and decay scheme of the neutral cascade provided the basis for assigning it to the baryon octet as a member of an isospin doublet. This assignment assumes the spin and parity, but the prediction has not yet been confirmed by experiment. Bubble chamber experiments have measured the neutral cascade mass (3, 19, 40, 66), lifetime (9, 18, 25, 37, 38, 40, 42), decay asymmetry parameters (9, 25, 40, 54), and production properties (9, 13, 25), but except for the mass the results are based on relatively few events.

In 1964 an experiment was planned by the High Energy Physics

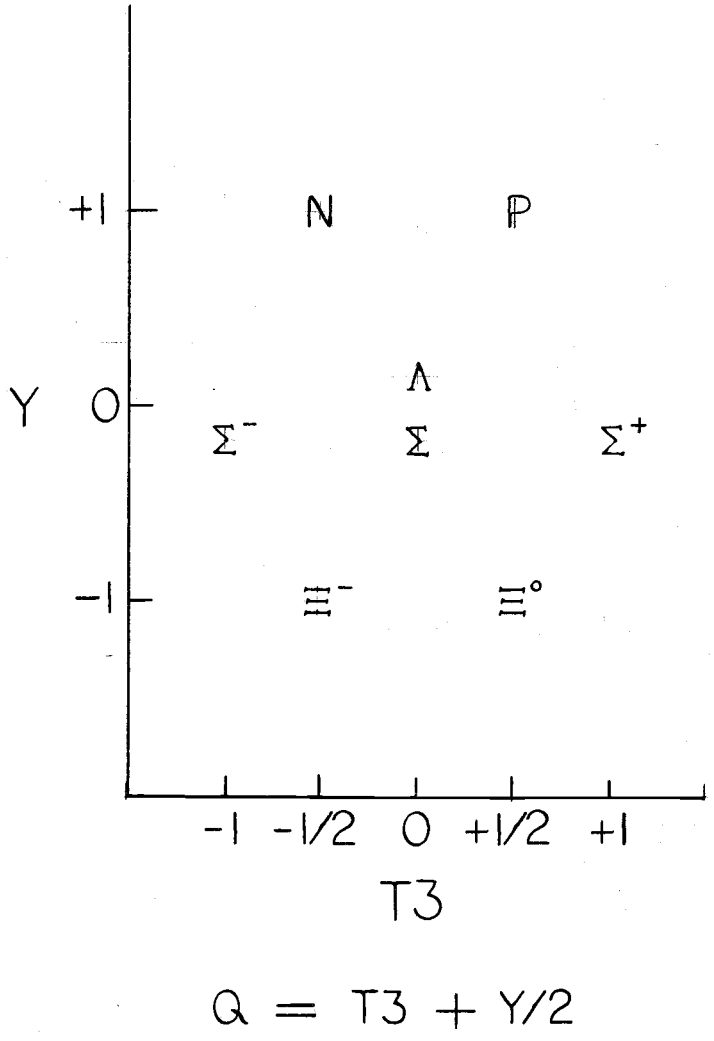

Figure 1. $1/2^+$ Baryon octet.

Group of the University of Washington to study the reaction:

$$k^- + p \rightarrow k^0 + \Xi^0$$

for a k^- momentum of 1.8 GeV/c. The decay of the k^0:

$$k^0 \rightarrow \pi^+ + \pi^-,$$

in addition to that of the cascade leads to four charged particles in the final state. By observing these particles along with the beam particle, one can completely determine the kinematics of an event and the observation of many events will yield the production differential cross section, the cascade polarization, and the decay asymmetry parameters. The first two numbers enter into a partial-wave analysis to determine the production amplitudes and the latter may be used to test certain theories concerned with weak interactions.

The proposal to do such an experiment was submitted in the Fall of 1964 and envisioned the use of spark chambers so as to acquire data at a considerably faster rate than was possible in bubble chamber experiments. By using scintillation counters to detect the signature of the reaction of interest, it would be possible to trigger the spark chambers upon the occurrence of a good event and thus be able to handle a beam consisting of several thousand particles per pulse.

Construction of the experimental apparatus began in 1965 and

in June 1966 setup and testing were initiated at the Bevatron, the University of California's proton synchrotron located at the Lawrence Radiation Laboratory in Berkeley, California. The useful data were taken from February to May 1968 and analysis was completed in January 1970. In this thesis the essential elements of the experiment will be described and the method by which a differential cross section measurement was made will be explained. The significance of the result will be discussed and a comparison will be made with past experiments.

k^- BEAM

The first element of the experiment to be discussed is the incident beam of k^- mesons (kaons). The kaons, along with a much greater number of π mesons (pions) were produced by flipping a small target[3] into the path of the protons circulating within the ring of the Bevatron. The resulting proton-nucleon collisions gave rise to an enormous number of secondary particles with momenta depending on the production angle. In order to derive a monoenergetic beam of kaons, it was necessary to have a system that would capture particles of the correct charge and momentum, separate the pions from the kaons, and transport the latter to the experimental area. Such a system was designed by R. W. Williams and V. Cook of the University of Washington and is shown in Figure 2.

The pairs of quadrupole magnets captured and focused the negative beam in a manner analogous to that of a lens in geometrical optics. The quadrupole Q5 and the sextupole allowed for fine tuning under certain running conditions. The H-magnets employed a vertical field to bend the beam and thereby select a certain momentum for entrance into Q6. All of the magnets used were standard beam transport elements and their specific characteristics may be found

---

[3] The internal target was of copper and from the point of view of the beam was 1/4" wide, 1/32" high, and 4" deep.

Figure 2. Beam transport system.

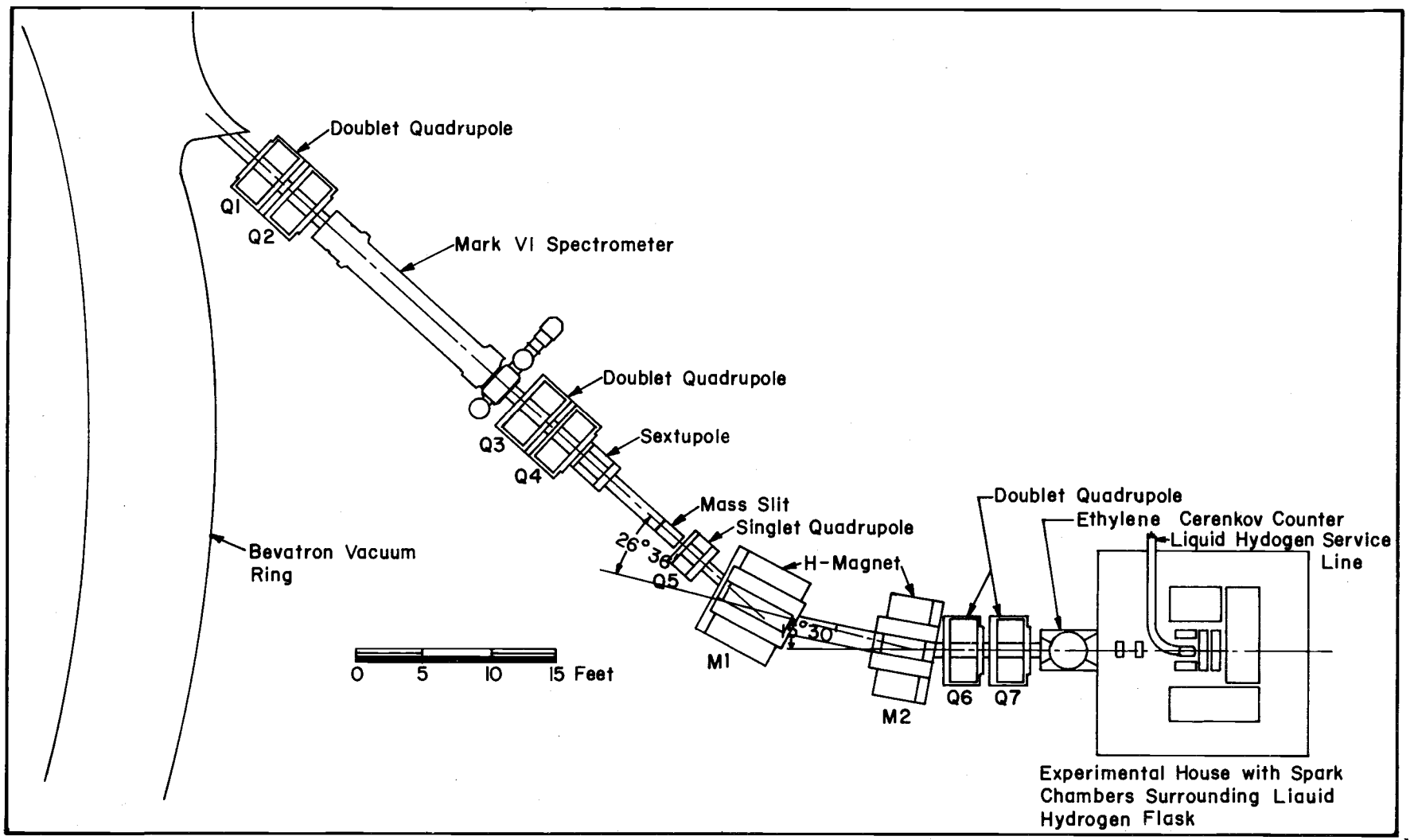
Doublet Quadrupole
Q1
Q2
Mark VI Spectrometer
Doublet Quadrupole
Q3
Q4
Sextupole
Mass Slit
Singlet Quadrupole
Q5
26° 36'
H-Magnet
M1
30'
M2
Q6
Q7
Doublet Quadrupole
Ethylene Cerenkov Counter
Liquid Hydogen Service Line
Bevatron Vacuum Ring
0 5 10 15 Feet
Experimental House with Spark Chambers Surrounding Liquid Hydrogen Flask

in (12).

The spectrometer used crossed electric and magnetic fields to differentially deflect particles on the basis of their speed. In practice, the spectrometer was set to allow kaons to pass through the "mass slit" which was a wedge-shaped gap formed by two blocks of uranium. The faster pions, on the other hand, missed the opening and were scattered or absorbed by the heavy material. Because of the finite momentum spread and directional divergences, the beam still consisted primarily of pions when it reached the experimental area. The flux was sufficiently low, however, that it was not necessary to remove these pions but only to identify each particle as it entered the target. This identification was provided by the ethylene-filled gas Cerenkov counter shown in Figure 3.

Effectively a beam particle entering the mylar window saw four tubes in a circle with one additional tube at the center. In principle, a kaon will emit Cerenkov light in a narrow cone seen only by the central tube while the pions have wider cones that intersect at least one of the outer tube faces.[4] The signals from the outer tubes were added together and put into anti-coincidence with the output of the central tube. Thus the Cerenkov counter was used to supply the logic signal $K\overline{\pi}$.

---

[4]The principles of Cerenkov radiation are presented in (43).

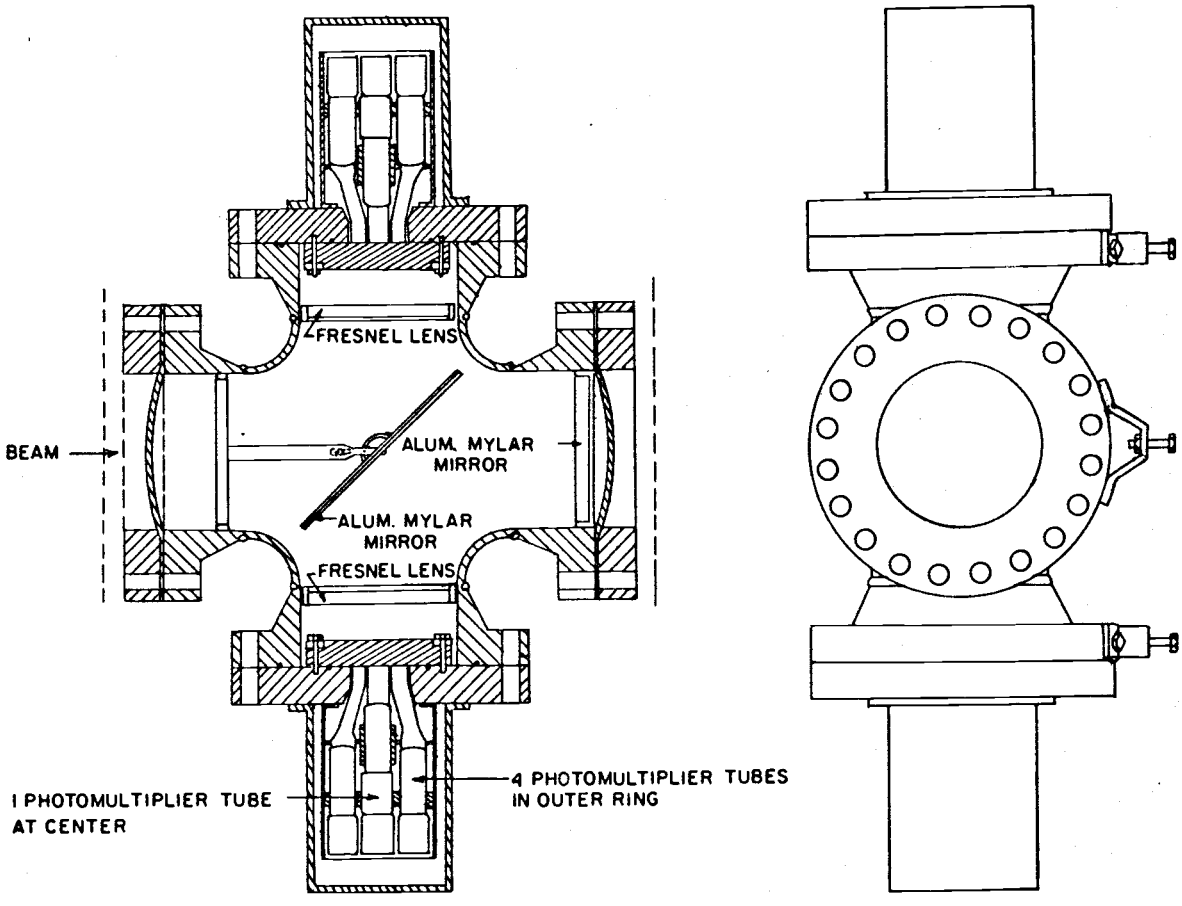

Figure 3. Cerenkov counter.

In addition to this identification, further beam definition was required to insure that the particle did in fact enter the target. Also, extra counters were needed to eliminate the possibility of accidental coincidences. Figure 4 shows the placement of these scintillation counters and Figure 5 shows their shapes and dimensions. Counter B' (the coincidence between B1 and B2) signaled the entrance of a particle into the Cerenkov counter. The array of counters H1-H4 was used to qualitatively measure the beam divergence, but since it subtended a greater solid angle than did B', little flux was lost by including it. The counter T1 was located inside the target vacuum chamber and was positioned directly in front of the liquid hydrogen flask. In order to absolutely define a parallel beam entering the target, an additional counter T1' was placed just in front of the vacuum chamber's mylar window. The flux passing through all of these counters was defined as the scintillation beam and yielded the logic signal

$$SBEAM = B' \cdot (H1+H2+H3+H4) \cdot T1 \cdot T1'.$$

To get a k signal, SBEAM was put into coincidence with the Cerenkov counter to yield

$$BEAM = SBEAM \cdot (K\bar{\pi})$$

which was a measure of the kaon flux.

The counters AA12 and AA3 bordered the H counters and T1',

Figure 4. Experimental layout.

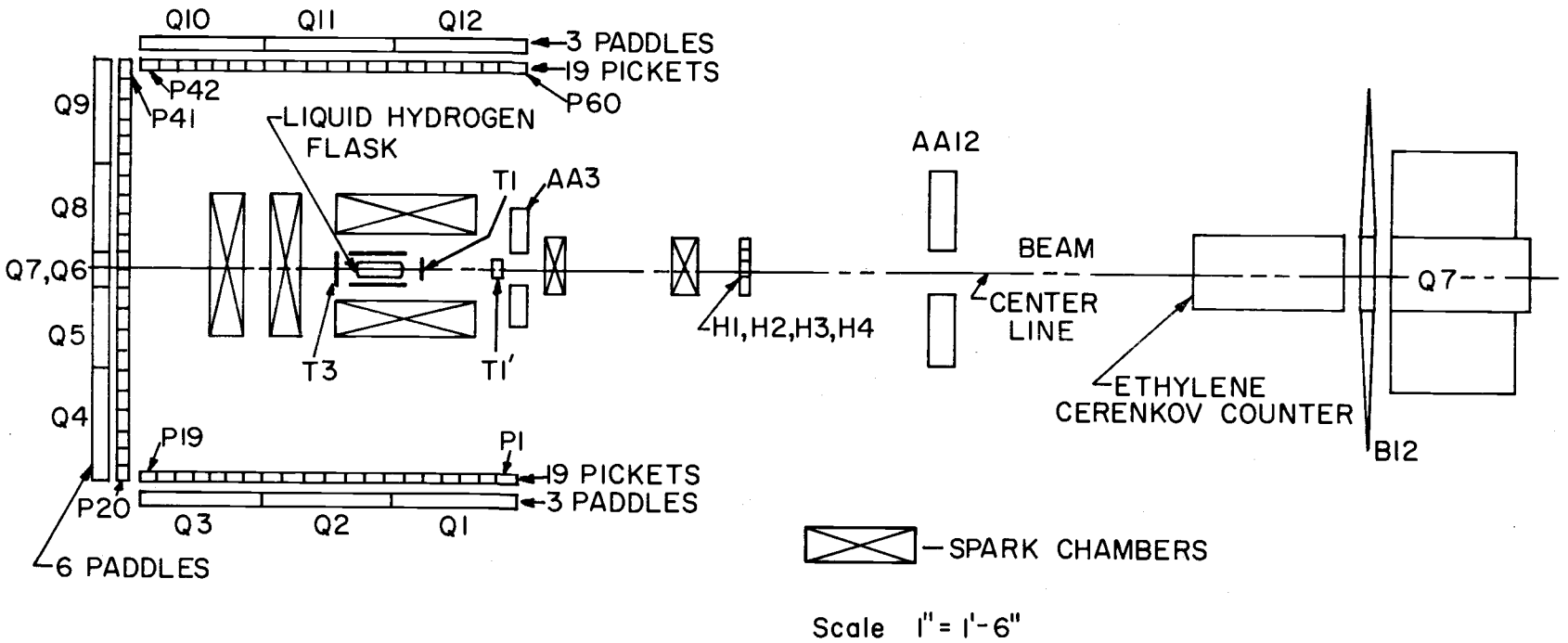
Q10
Q11
Q12
3 PADDLES
19 PICKETS
P42
P41
P60
Q9
LIQUID HYDROGEN
FLASK
AA12
TI
AA3
Q8
Q7,Q6
BEAM
Q7
Q5
CENTER
LINE
HI,H2,H3,H4
T3
TI'
Q4
ETHYLENE
CERENKOV COUNTER
P19
PI
B12
19 PICKETS
P20
3 PADDLES
Q3
Q2
QI
6 PADDLES
SPARK CHAMBERS
Scale 1" = 1'-6"

Figure 5. Beam defining counters.

B12

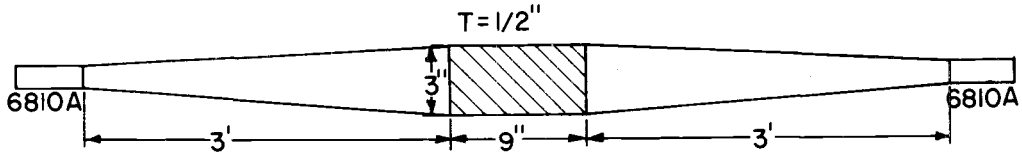

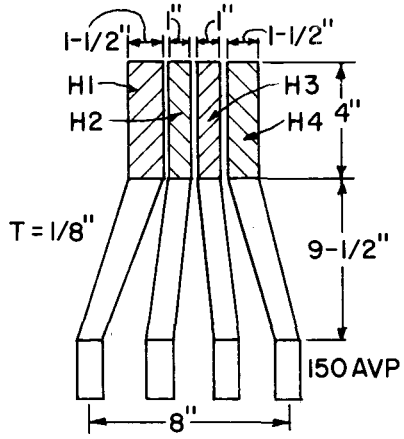

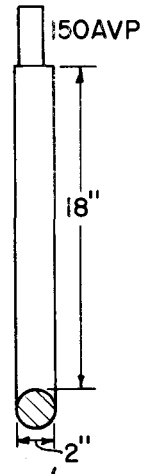

T1'

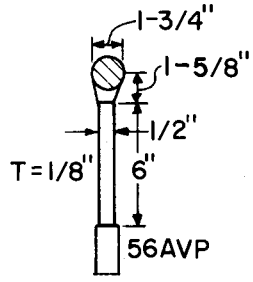

T1

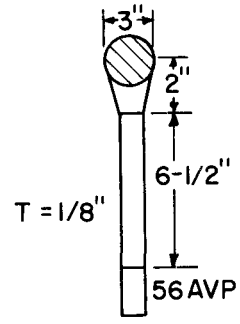

T3

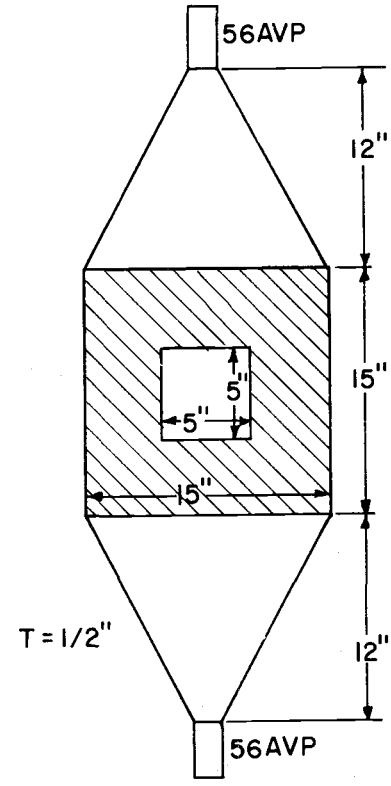

AA12

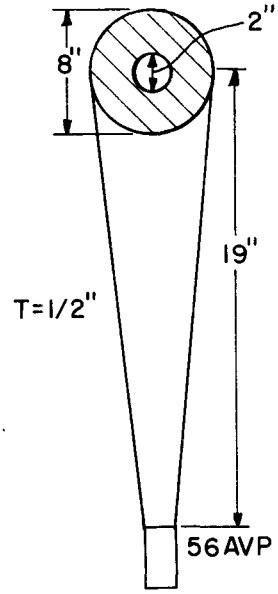

AA3

T = Thickness

respectively. Their function was to veto cases in which divergent beam particles triggered the "yes" counters by emitting Cerenkov radiation while passing through the light pipes joining the scintillators to the photomultiplier tube faces. The complete logic signal, then, that indicated a kaon entering the target was

$$\text{ABEAM} = \text{BEAM} \cdot \overline{\text{AA12}} \cdot \overline{\text{AA3}}.$$

Typical counting rates for the various beam elements as well as operating details for the spectrometer and Cerenkov counter will be given in Chapter 8.

LIQUID HYDROGEN TARGET

A liquid hydrogen target was used to avoid k^--n interactions and to eliminate the corrections necessary when the target particle is bound within a nucleus. In this experiment the cylindrical target flask was six inches long and two inches in diameter. Multiplying the length by the density of boiling liquid hydrogen gives an effective interaction length of about one gm/cm^2. To slow the loss of target material and for safety reasons, the flask was supported within a vacuum chamber (Figure 6). The main stock of liquid hydrogen was maintained in a reservoir located outside the experimental house and connected to the flask by a long fill line. The reservoir was filled from large dewars supplied by the Target Group which built the hydrogen target according to specifications and assembled the auxiliary equipment.

Located within the vacuum chamber were three scintillation counters, two of which were actually used. Counter T1 was part of the beam system and has been described in Chapter II. Counter T3 was a disk-shaped counter (Figure 5) and was located just downstream from the flask. The purpose of this counter was to veto events in which charged particles were produced by the k^--p interaction. By putting the signal from T3 into anticoincidence with the beam signal, a neutral beam was defined:

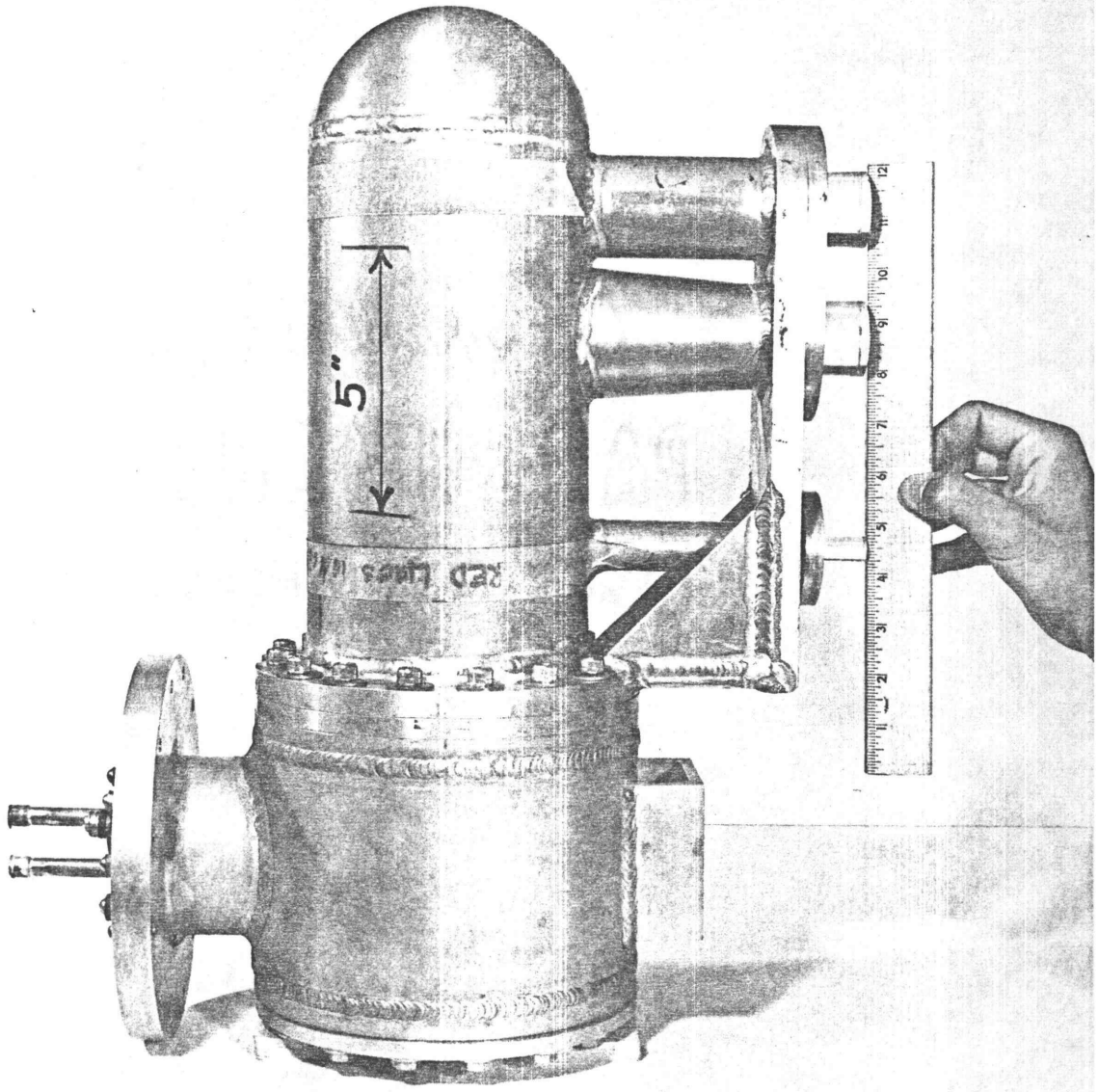

Figure 6. Liquid hydrogen target.

$$NBEAM = ABEAM \cdot \overline{T3}.$$

Now since the cross section for charged particle production exceeds that for the production of neutrals by a factor of 2.5, it was essential that T3 be a very efficient counter to avoid being overwhelmed by backround events. As measured during the experiment, the efficiency of T3 varied between 99.5% and 99.8%. These values were none too high, and combined with the fact that T3 was limited in size led to a considerable number of charged events slipping through. The seriousness of this effect was reduced somewhat by counting the number of charged particles in the final state. The hodoscope, described in the next chapter, demanded that four charged particle be present to signal a good event.

HODOSCOPE

As was mentioned in the introduction, the reaction of interest leads to a four charged particle final state. To distinguish this state from, say, the charge exchange final state, a hodoscope was constructed to count the number of charged particles passing through the spark chambers. This hodoscope was an array of 60 vertical "picket" scintillation counters backed up by 12 "paddle" counters. The dimensions of these counters are given in Figure 7, while their layout is shown in Figure 4. As designed, the picket array would be sufficiently discrete so that each charged particle would pass through a different counter. The pulses from all counters could then be simply added to give the multiplicity of the final state. The paddle counters were used to "gate" the signals from the pickets. By allowing the latter to pass only when the appropriate paddle had been triggered, an effective coincidence was obtained.

It was important that the detection efficiency be uniform along the entire four foot length of the pickets, and some consideration was given to mounting a photomultiplier tube on both ends of the counter. After testing several models, however, it was found that a single Amperex 150 AVP performed quite satisfactorily. An electrical base (Figure 8) was designed to supply sufficient current during the beam pulse and divider boxes were constructed to allow the high

Figure 7. Hodoscope counters.

ALL COUNTERS 1/2" THICK

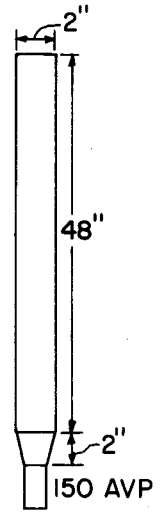

ALL PICKETS
EXCEPT 29-32

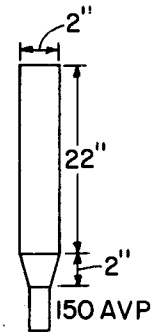

PICKETS
29-32

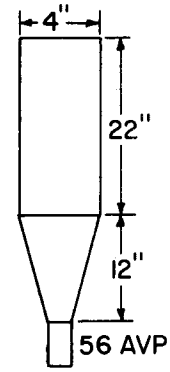

PADDLES
6 and 7

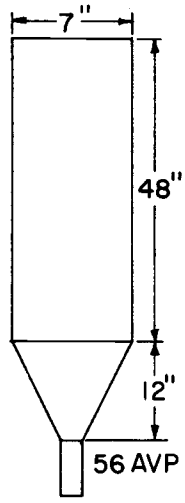

PADDLES
5 and 8

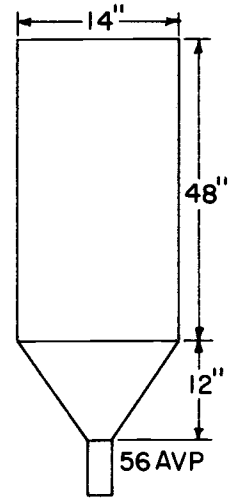

PADDLES
1-4 and 9-12

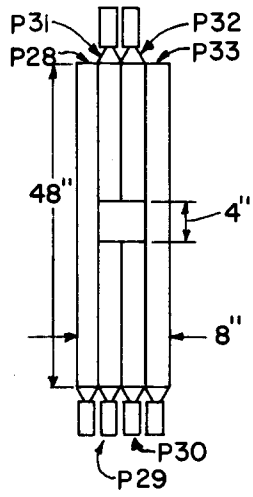

CENTER PORTION OF THE
DOWNSTREAM WALL OF
THE HODOSCOPE

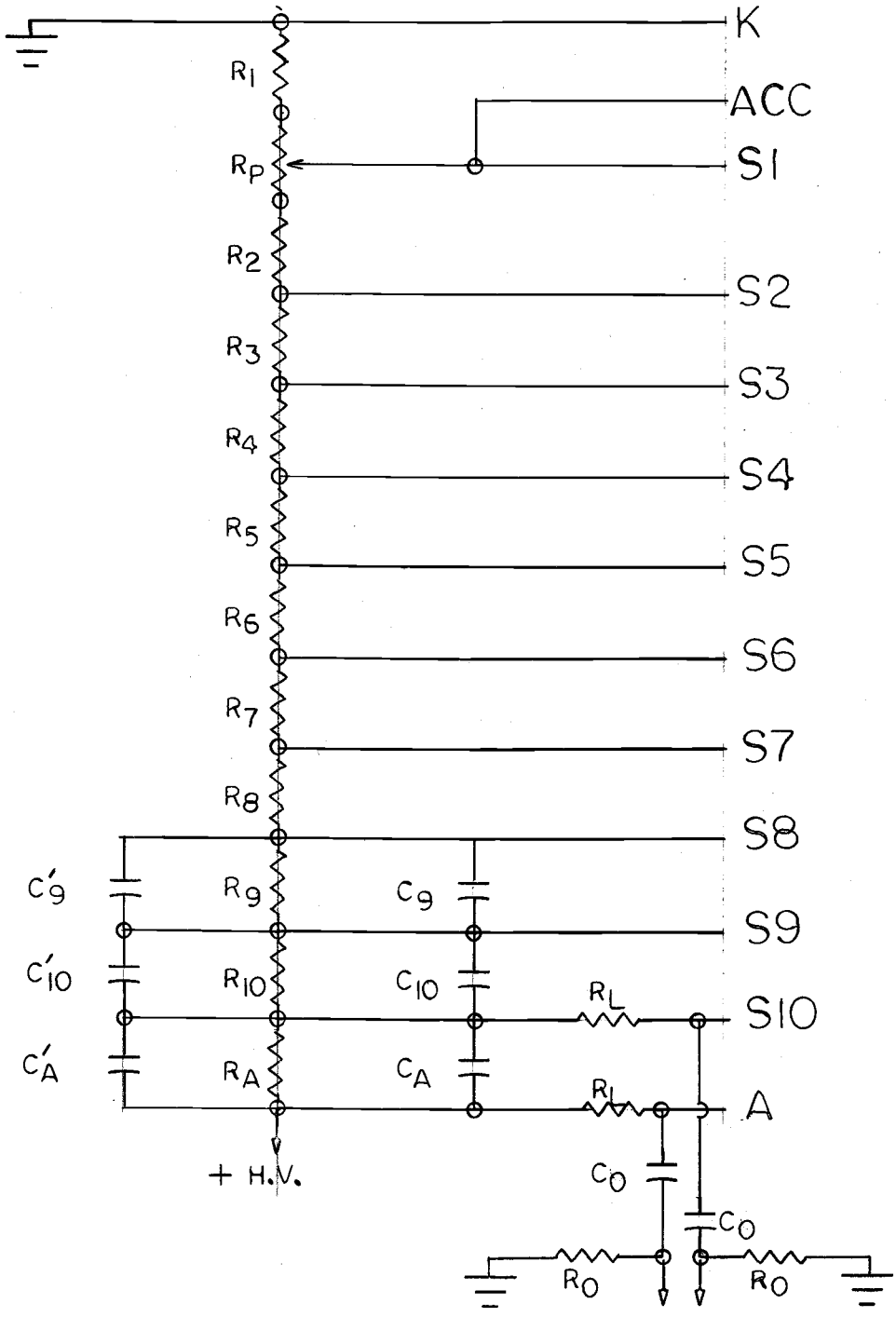

Figure 8. Amperex 150 AVP tube base.

voltage applied to the tubes to be individually adjusted. About 75 units consisting of a picket, an electrical base, and a divider box were built and tested at the University of Washington. The paddles were equipped with Amperex 56 AVP tubes and with bases and divider boxes used in a previous experiment.

Before using any of the counters, it was necessary to find the optimal high voltage setting for them. This was accomplished by plotting efficiency against voltage and determining at which voltage the efficiency reached a plateau. The efficiency was measured by placing the counter to be tested between a pair of counters ("telescope") and recording the triple coincidence rate as well as the double coincidence rate between the telescope counters. The ratio triples:doubles is independent of the telescope counter efficiencies and may be defined to be the efficiency of the counter being tested. The setup and a typical curve are shown in Figure 9.

In spite of occasional light leaks, broken glue joints, misplaced cables, and faulty tube bases, the hodoscope operated in a quite uniform manner and gave an accurate count when from one to five particles passed through it. The logic signal from the hodoscope was labeled $\propto$, and in coincidence with NBEAM constituted the "good event" signal which was used to trigger the spark chambers described in the next chapter.

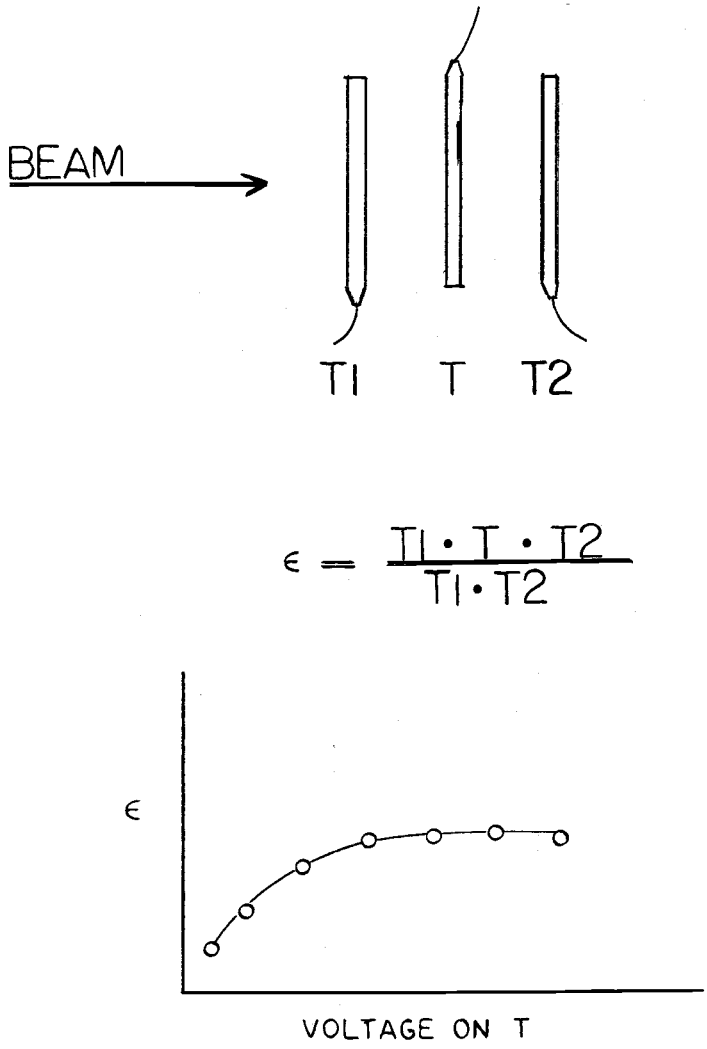

Figure 9. Plateau of a scintillation counter.

SPARK CHAMBERS

Two types of spark chambers were run during the experiment, but the data from one type were not used in the analysis and so will not be discussed in any detail here. In the top view of the experiment (Figure 10), three large spark chambers (with their mirror views as well) may be seen situated outside of the hodoscope. The plates of these chambers were of steel and were designed to detect the gamma rays from the neutral pion decay by converting them into electron pairs. Now by demanding the presence of gamma rays, one could certainly eliminate backround events, but this was not done because of uncertainty about the biases introduced by casting out good events. Since not enough was known about the efficiencies and operating characteristics of the steel chambers, the information provided by them was not utilized in this first analysis of the data.

The other type of spark chamber had aluminum foil plates sandwiched between plexiglass frames and with mylar sheets on the outside to make them gas-tight. Figure 4 shows the arrangement of these spark chambers: two "beam" chambers (Figure 11) detected the incident k^- particle and four "V" chambers (Figure 12) hopefully contained the decay products of the Λ and k^0. The beam chambers had six one-quarter inch gaps with an effective cross sectional area of 5" x 5". The V chambers were 20" x 20" with 12 one-quarter

Figure 10. Camera view of the experiment.

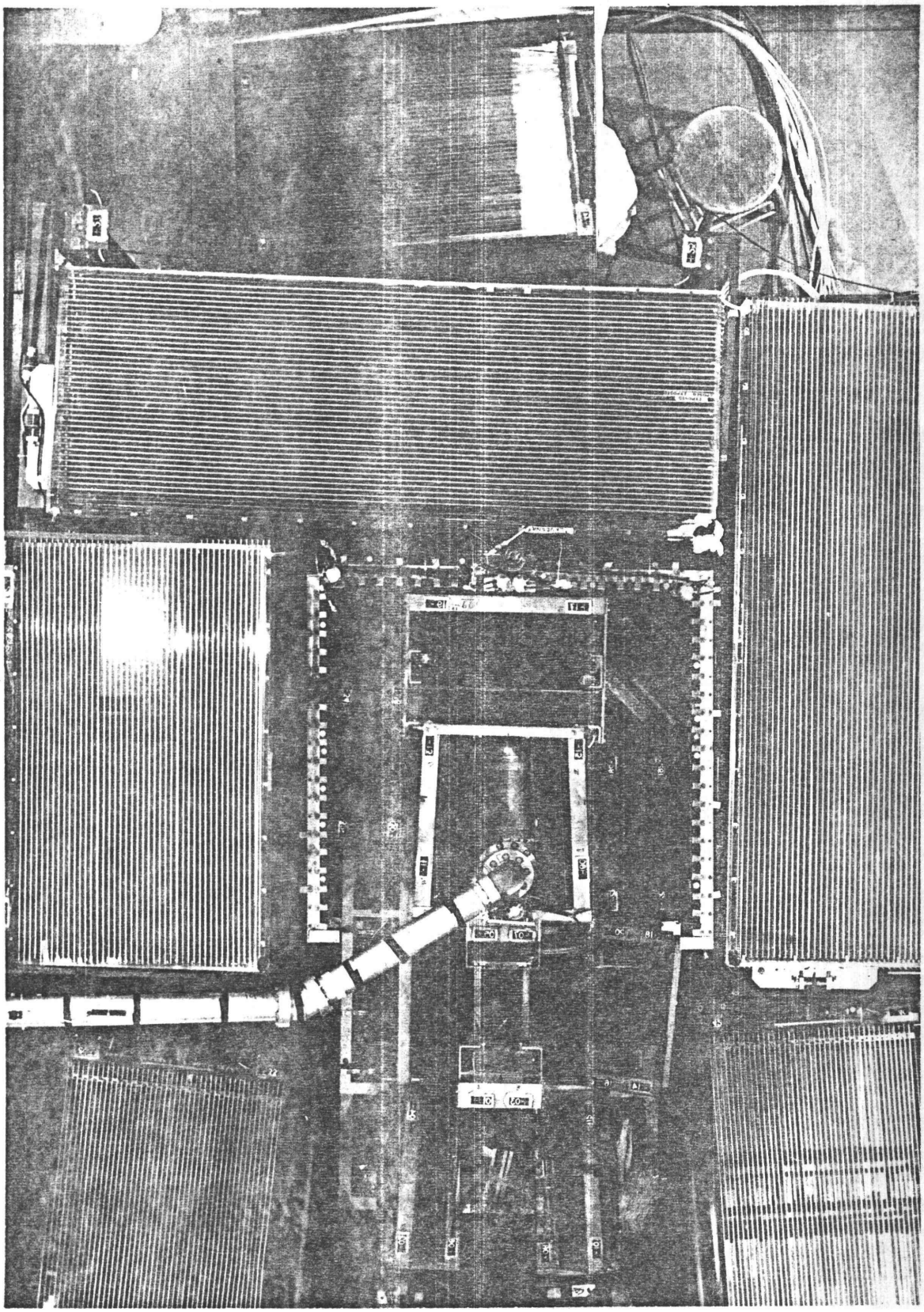

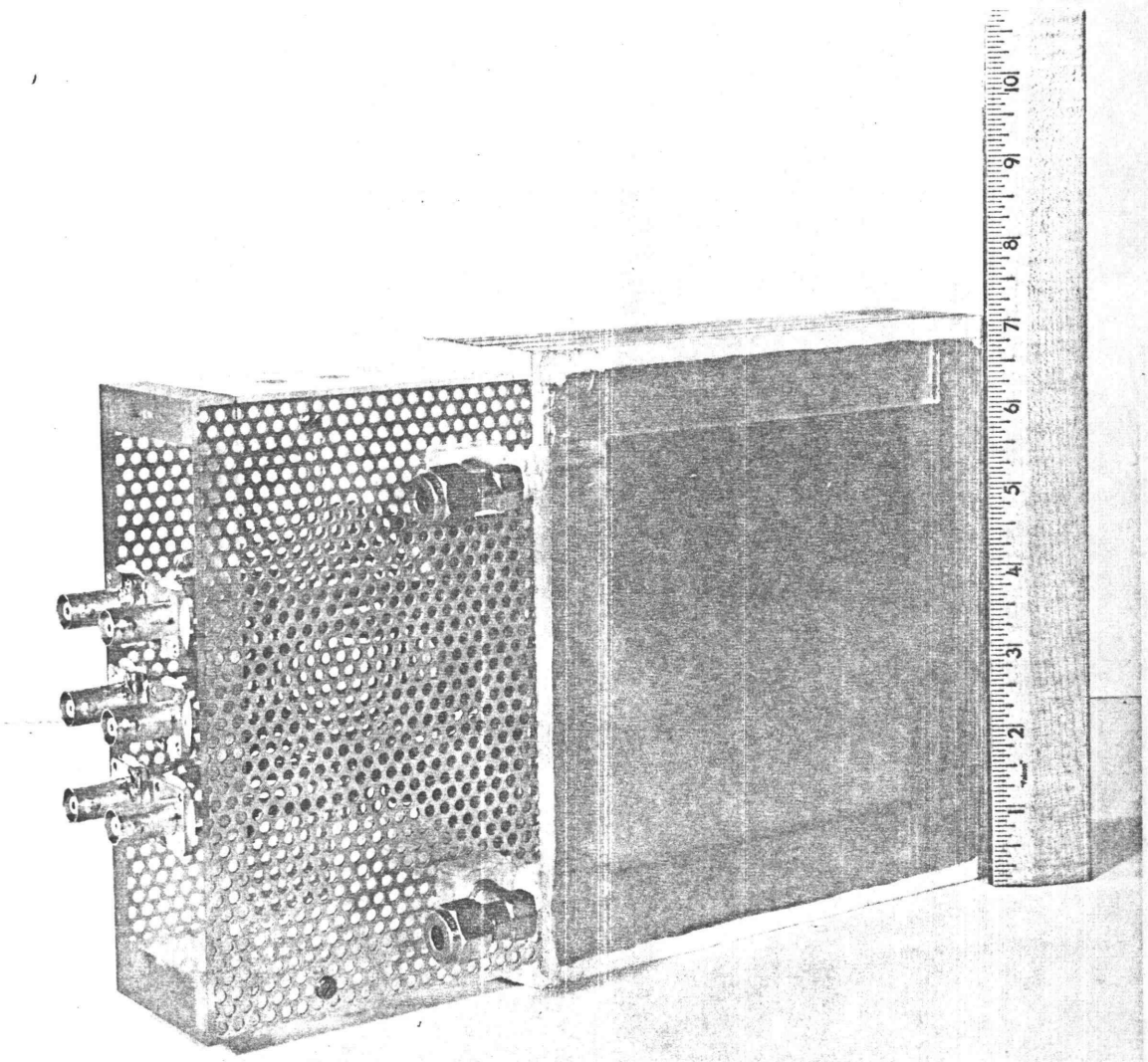

Figure 11. Beam spark chamber.

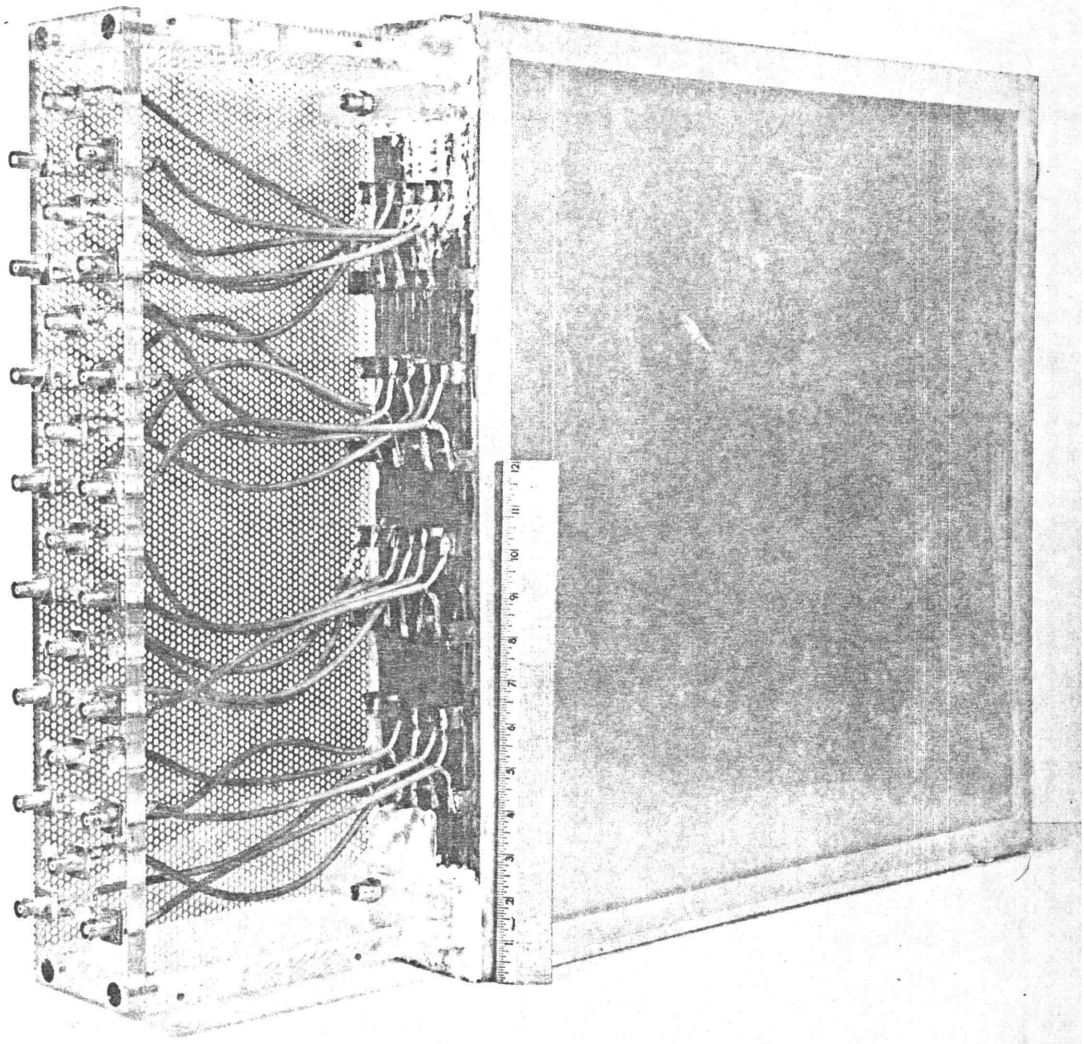

Figure 12. V spark chamber.

inch gaps. All of these chambers operated on Neon which was contained within a recirculating system. The system was built around three pumping carts which contained liquid nitrogen traps to remove impurities.

Alternate plates of each spark chamber were driven to a high voltage upon the electrical breakdown of spark gaps[5] located outside of the experimental house (Figure 13). A schematic drawing of a spark gap and transformer are given in Figure 14, while the overall distribution system is shown in Figure 15. The initiating signal which triggered the spark chambers came from an EG&G logic module which provided an output when fed a "good event" signal from the beam and hodoscope electronics. In the next chapter the means by which the resulting sparks were photographed will be discussed.

---

[5] The spark gap is effectively a switch which can be closed in nanoseconds.

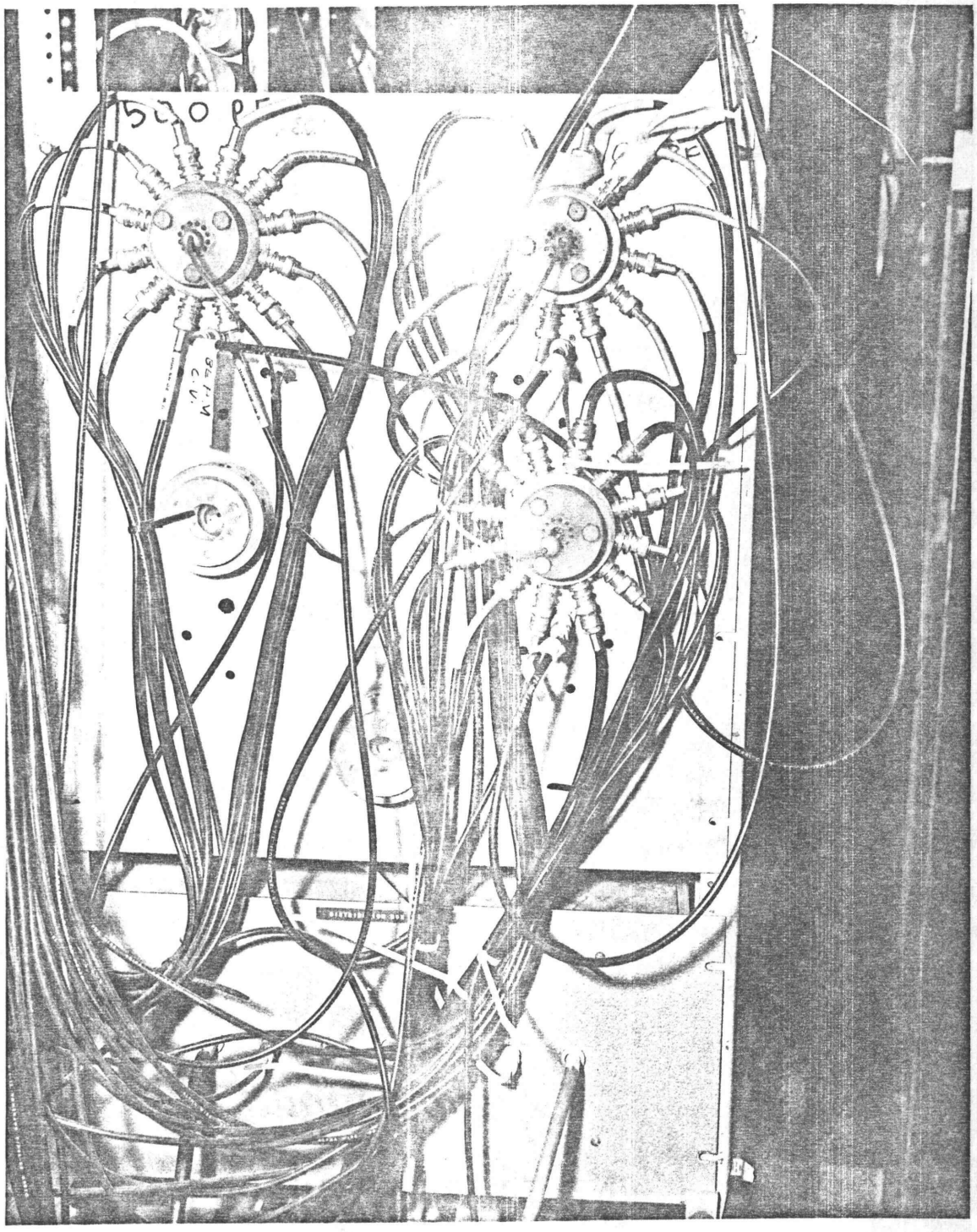

Figure 13. Spark gaps.

Figure 14. Foil chambers spark gap.

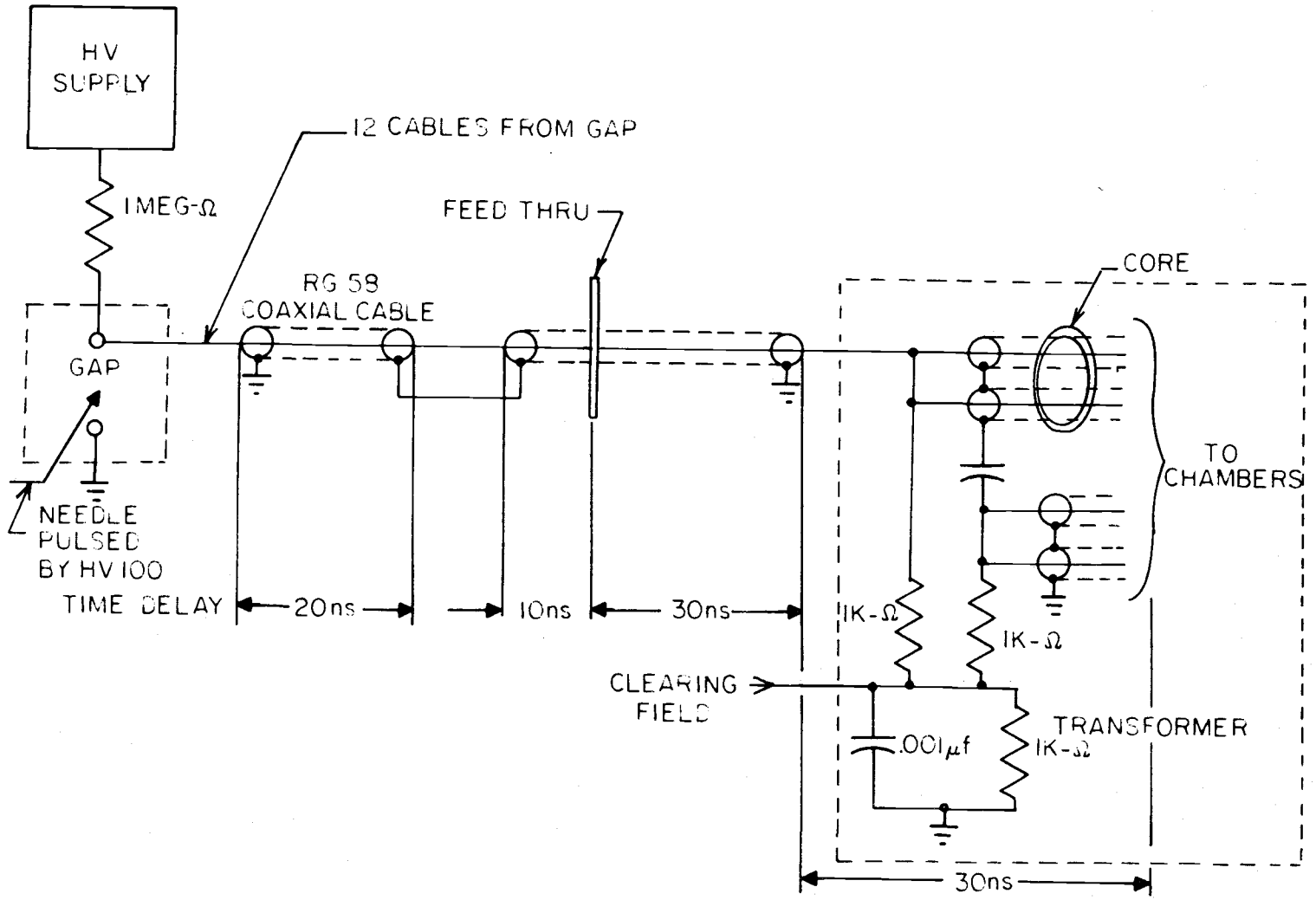
HV
SUPPLY
1MEG-Ω
12 CABLES FROM GAP
FEED THRU
RG 58
COAXIAL CABLE
CORE
GAP
NEEDLE
PULSED
BY HV 100
TIME DELAY
20ns
10ns
30ns
TO
CHAMBERS
1K-Ω
1K-Ω
CLEARING
FIELD
.001μf
TRANSFORMER
1K-Ω
30ns

Figure 15. High voltage distribution system for spark chambers.

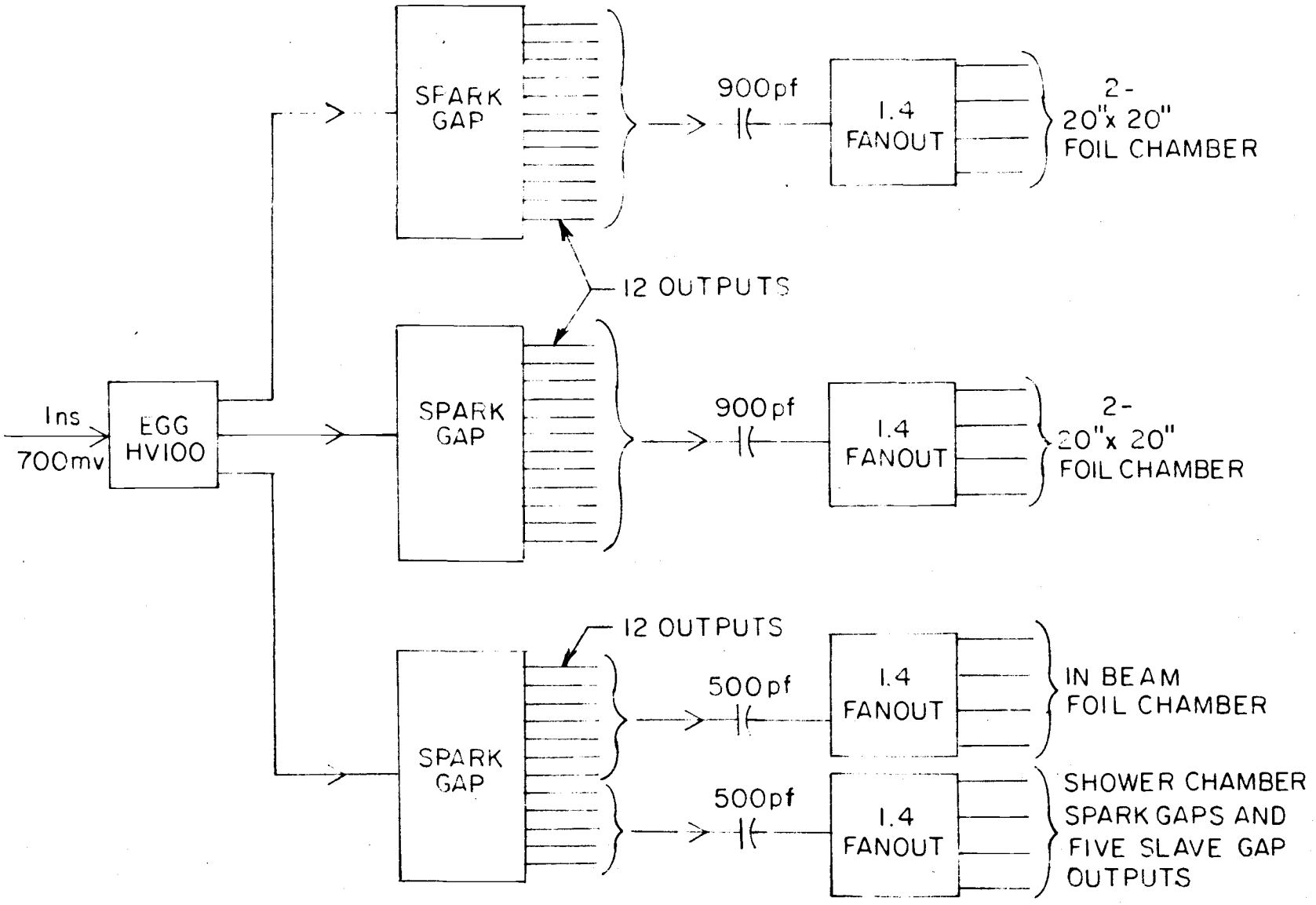
Ins
700mv
EGG
HV100
SPARK
GAP
SPARK
GAP
SPARK
GAP
12 OUTPUTS
12 OUTPUTS
900pf
900pf
500pf
500pf
1.4
FANOUT
1.4
FANOUT
1.4
FANOUT
1.4
FANOUT
2-
20"x 20"
FOIL CHAMBER
2-
20"x 20"
FOIL CHAMBER
IN BEAM
FOIL CHAMBER
SHOWER CHAMBER
SPARK GAPS AND
FIVE SLAVE GAP
OUTPUTS

CAMERA AND OPTICS

In order to record the spark chamber tracks on film, cameras were mounted in an alcove above and off to the side of the experimental apparatus. As shown in Figure 16, four cameras were used to permit the exposure of four frames during a single beam pulse. Relatively inexpensive Beattie backs were sufficient since there was then no need for a rapid film advance. The figure also shows the pyramid which reflected the image of the experiment into the lenses. Figure 10 is an actual photograph taken during the running. To view the entire experiment, 70 millimeter film was employed and a long optical path was obtained by mounting a large mirror some 23 feet above the floor of the experimental house.

The reconstruction of spark chamber tracks requires a stereo view of the chambers. The overhead mirror recorded the top view directly, but other mirrors were needed to project the side views upward. In addition to the sparks, certain reference marks or fiducial marks were also photographed. Physically, the fiducials consisted of a small box with a bulb to illuminate an etched glass plate. As may be seen in Figure 10, each plate carried an identifying number and a cross which could be surveyed. The fiducials were used to set up the transformation between film space and real space; details will be presented in Chapter X.

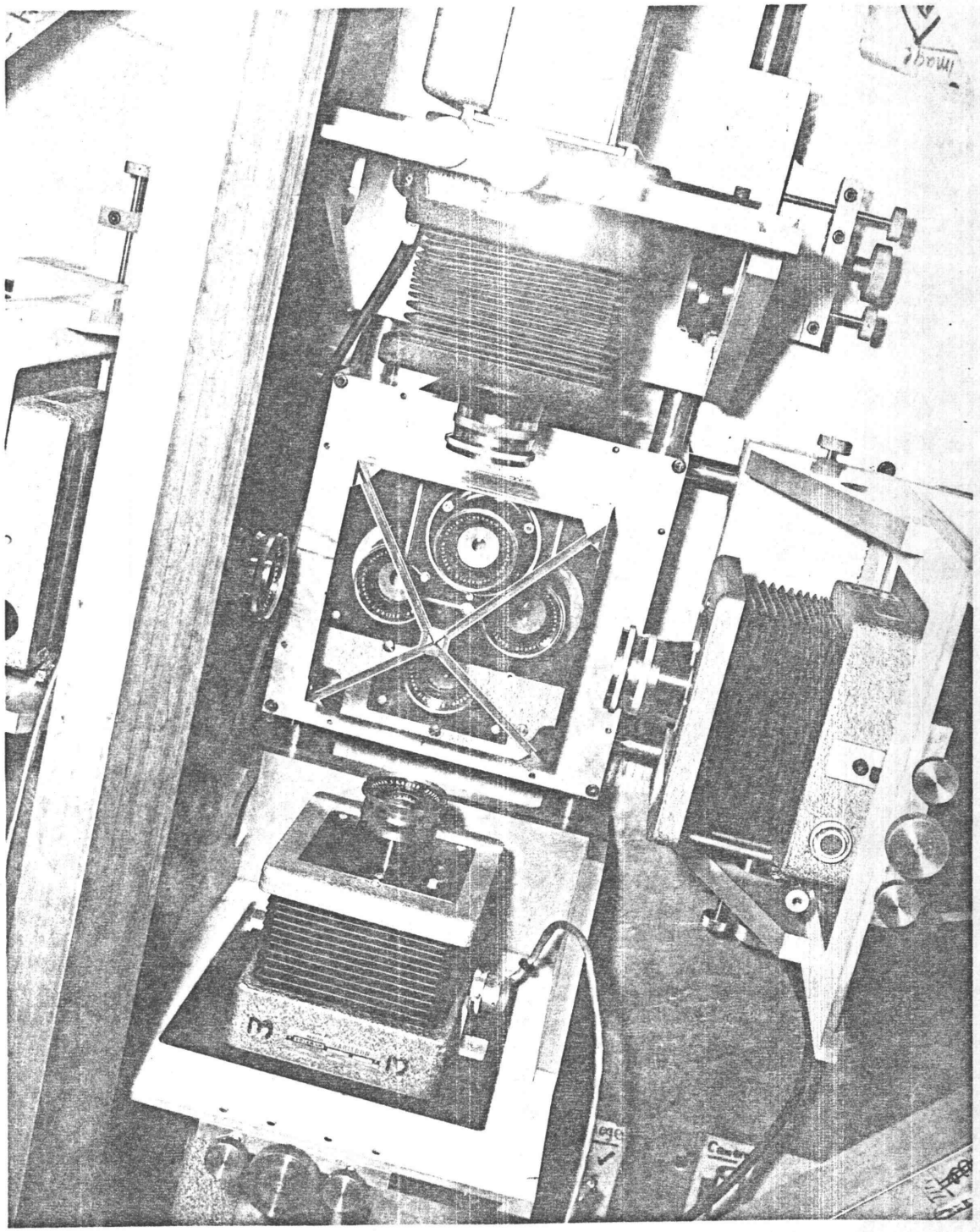

Figure 16. Camera system.

ELECTRONICS

Electronic devices were used in the experiment to control the cameras and fiducials, to process the signals from the photmultiplier tubes, to trigger the spark chambers, and to perform other miscellaneous tasks. Nearly all of the electronics were contained in commercially-built modules that were purchased or borrowed for use in this experiment.

The "slow" electronics operated on a microsecond or longer time scale and governed the experiment over the period of one accelerator cycle. One circuit integrated the signals from a beam counter and displayed flux vs time on a cathode ray tube. The experiment was gated off during spikes in this display so that multiple tracks would not appear in the beam spark chambers. Another 40 millisecond gate was applied after each good event signal to give the camera shutters time to operate and the spark chamber capacitors time to recharge. The slow electronics also flashed the fiducials, operated the shutters, and then advanced the film at the end of each beam pulse.

The "fast" (nanosecond) electronics modules were used to process the photomultiplier tube signals. This speed was necessary to differentiate between pulses due to the passage of a charged particle and those coming from electrons thermally ejected from the

photocathode. By requiring a close coincidence between signals from successive counters, triggers resulting from two noise pulses could be eliminated because of the relatively slow rate of generation of such pulses.

Each signal from a photomultiplier tube first entered a discriminator which ignored amplitudes below 100 millivolts and provided a standard output pulse for higher input amplitudes. Other electronic modules functioned as coincidence circuits, adders (mixers), and gates. Block diagrams of the beam and hodoscope electronics logic are shown in Figures 17-21. The good event signal which was the output of the final discriminator triggered a pulser which led to the spark gaps and thus caused the firing of the spark chambers. Other outputs led to the slow electronics and to a scaler for counting purposes. Details about the tuning of certain portions of the electronics may be found in (39) and in the next chapter typical running conditions will be described.

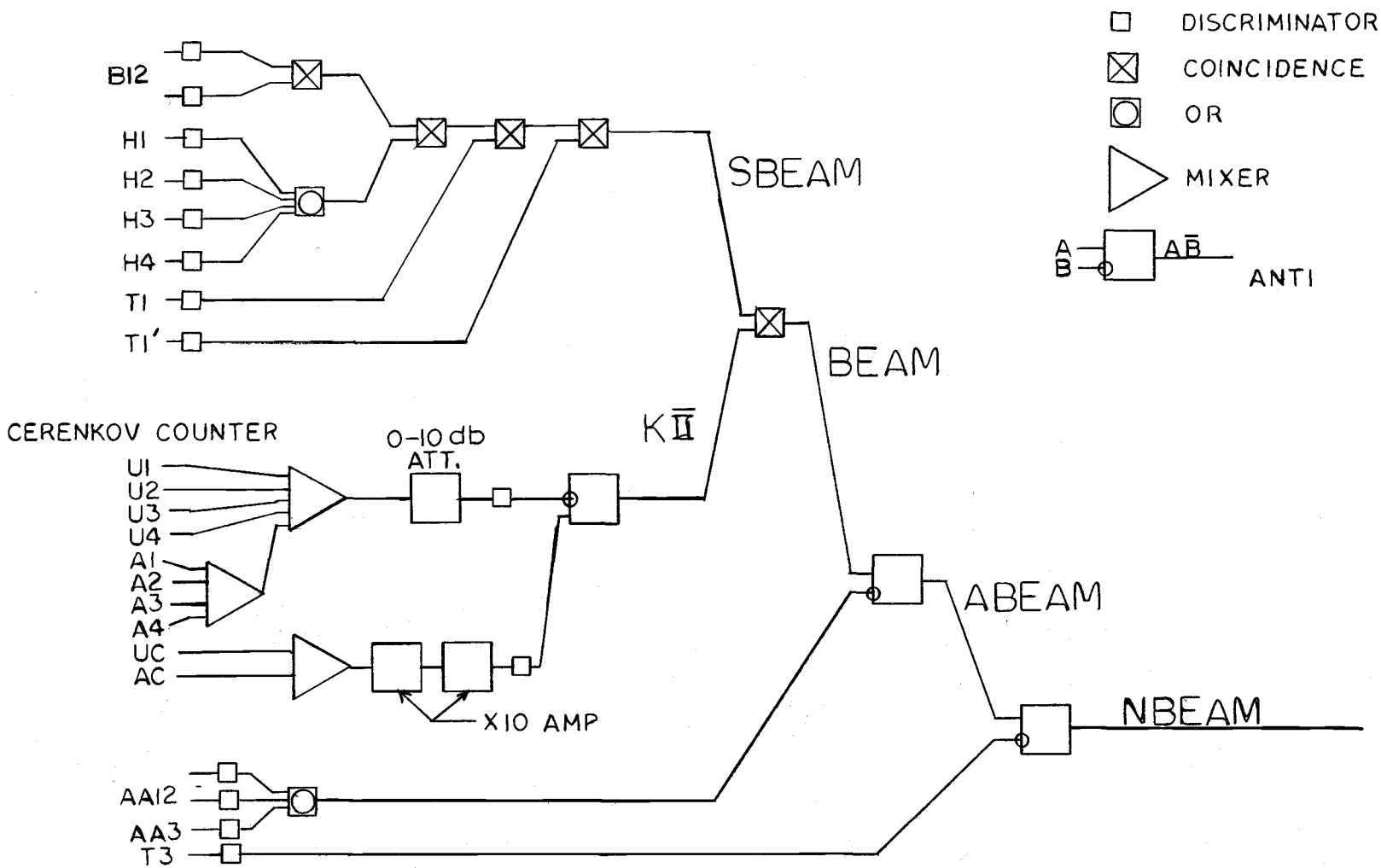

Figure 17. Beam electronics.

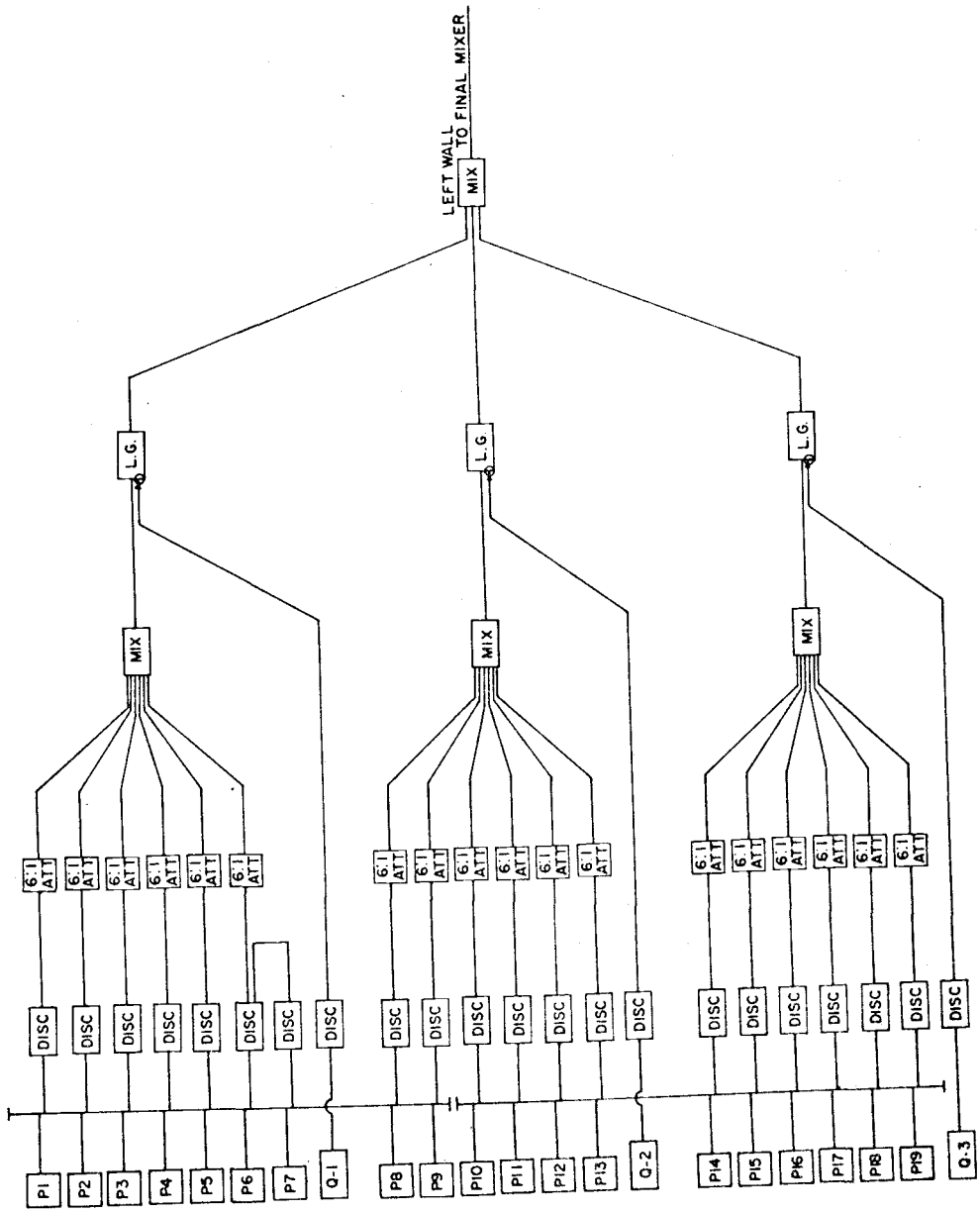

Figure 18. Hodoscope left wall electronics.

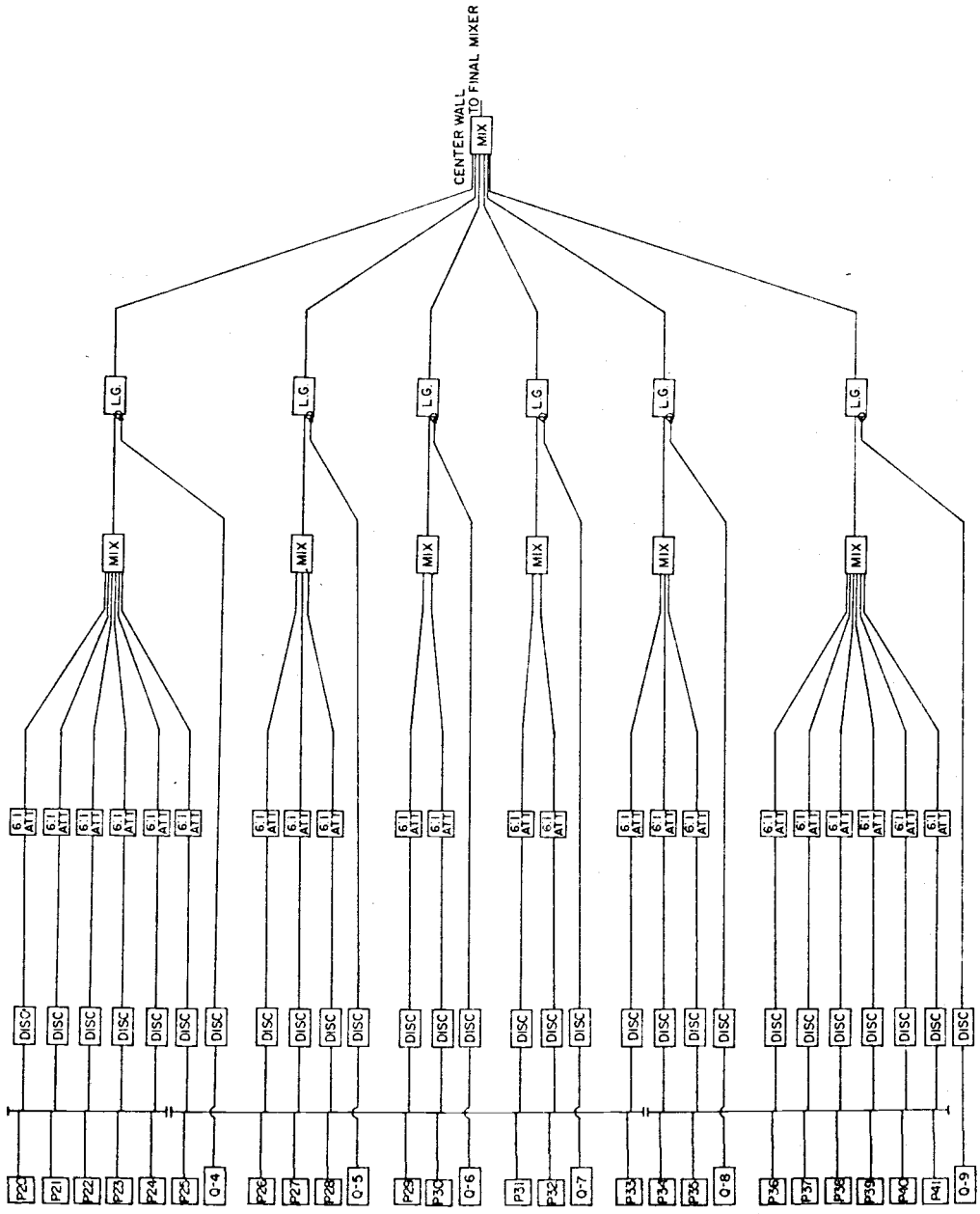

Figure 19. Hodoscope center wall electronics.

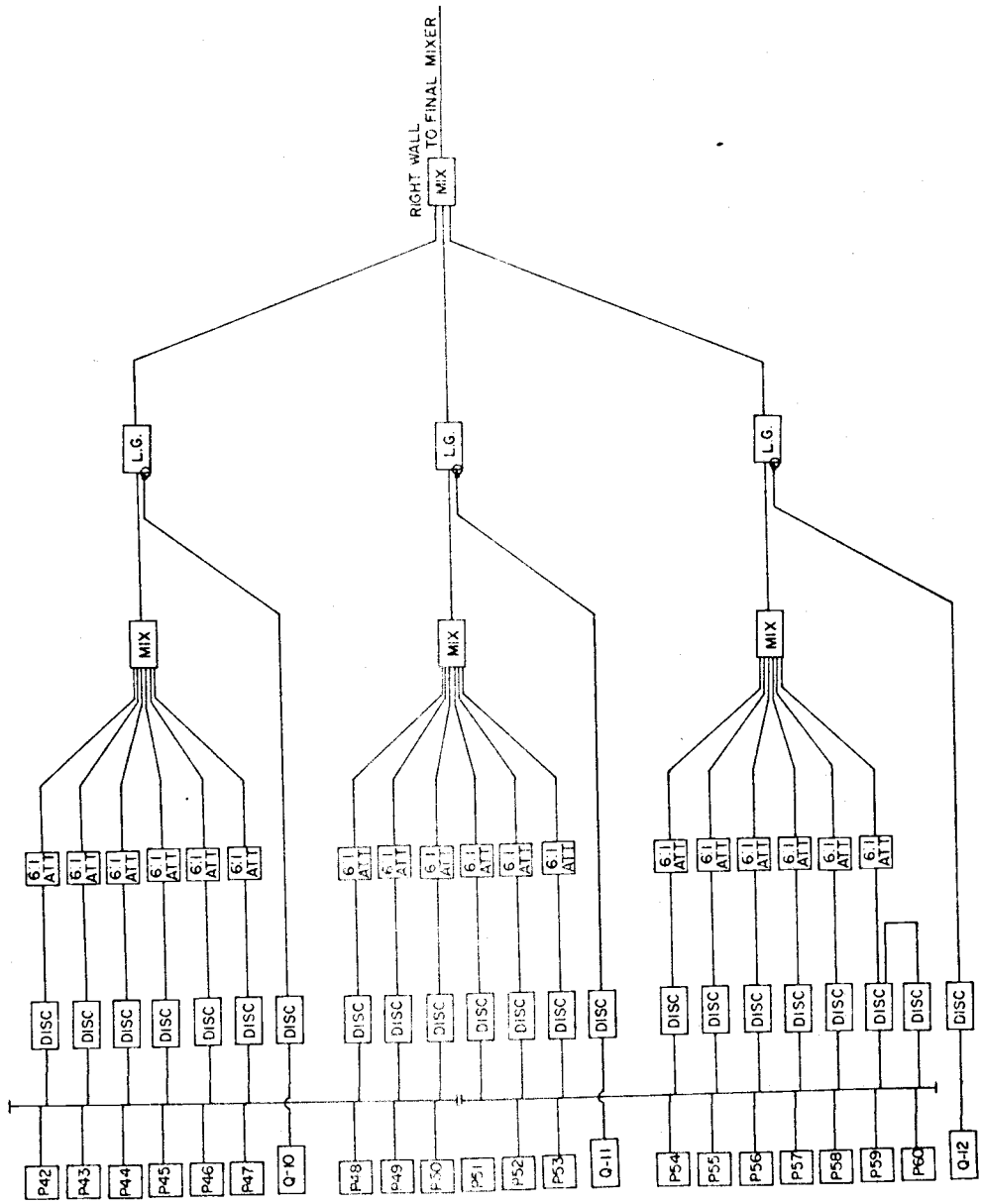

Figure 20. Hodoscope right wall electronics.

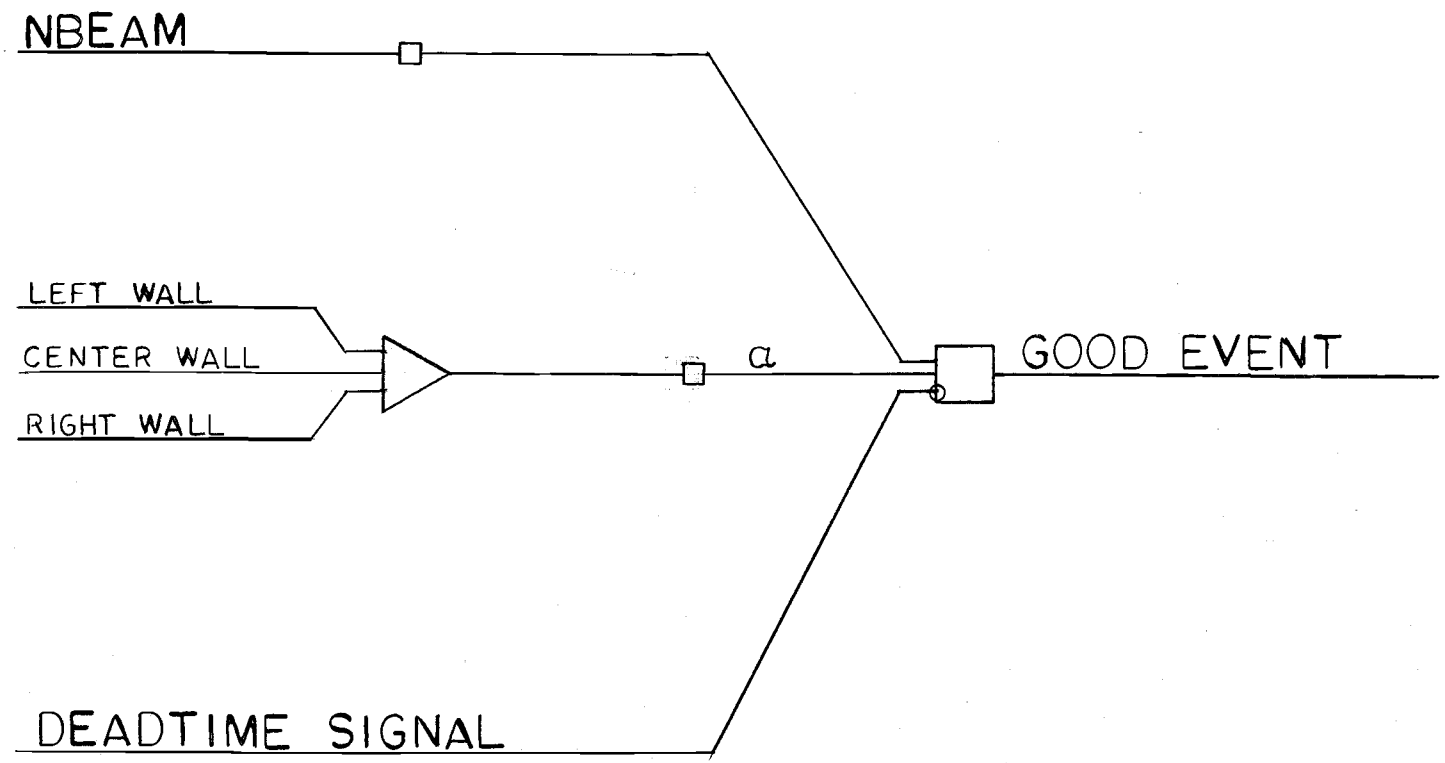

Figure 21. Final stage of electronics.

DATA TAKING

The data were accumulated during a series of runs consisting of from two to seven days of primary control over the Bevatron running conditions. During these periods the University of Washington group set the Bevatron energy, spill time, and flux to maximize the number of beam particles while also allowing other groups to carry on experiments. The machine operated 24 hours per day and three shifts of two persons each were used during the running. In this chapter the important aspects pertaining to the prepration for and carrying out of a run will be described.

Prior to the data taking several running periods were devoted to finding the optimal Bevatron energy at which to flip the internal target as well as the best radial and azimuthal settings for this target. The criterion used in each case was the number of kaons per pulse incident on the hydrogen target. The accuracy of this number depended critically on the proper operation of the Cerenkov counter and the velocity spectrometer. Consequently, the calibration of these two instruments will be discussed next.

The variable parameter related to the Cerenkov counter was the pressure of the ethylene gas which determined the index of refraction, n, of the medium. The emission angle, θ, of Cerenkov light depends on n through the relation $\cos\theta = c/vn$ where c is the speed

of light in a vacuum and v is the particle velocity. Raising the pressure increased n and thus also the emission angle. The plot of flux vs pressure shown in Figure 22 illustrates the effect of an emission angle change on the counting rates of the various tubes. At low pressure the slow kaons do not radiate and the pions are detected only by the central tube, which results in pseudo - k^- signals. As the pressure is increased the pion Cerenkov light begins to strike the outer tube faces and the k^- rate is reduced. At the optimum pressure setting the kaons emit light into the central detector and the counting rate increases once again. Since the pressure is temperature dependent, a recalibration was necessary from time to time throughout a run.

Within the velocity spectrometer both the electric and magnetic fields could be varied, but the former was essentially fixed and calibration was accomplished by adjusting the magnet. Figure 23 shows the variation of the kaon and pion fluxes with current through a magnet shunt. The spatial separation between the kaons and pions was very small and the magnetic field had to be carefully set to cause the pions to miss the mass slit. Maximizing the number of kaons was not the sole concern, since it was also essential to limit the ratio of pions to kaons. Under optimum conditions this ratio was about five to one, but constant adjustment of the spectrometer was required to maintain it.

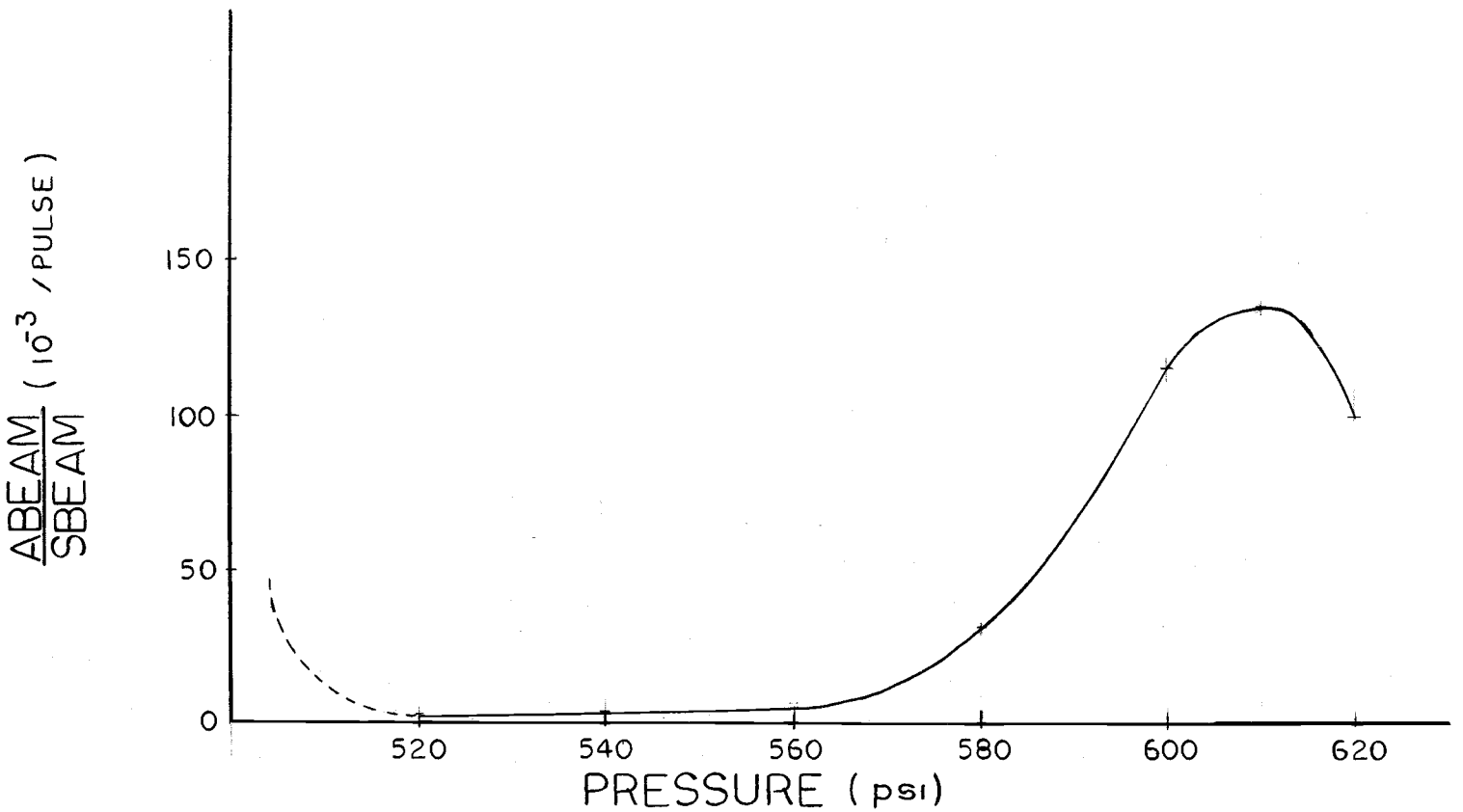

Figure 22. Cerenkov counter pressure curve.

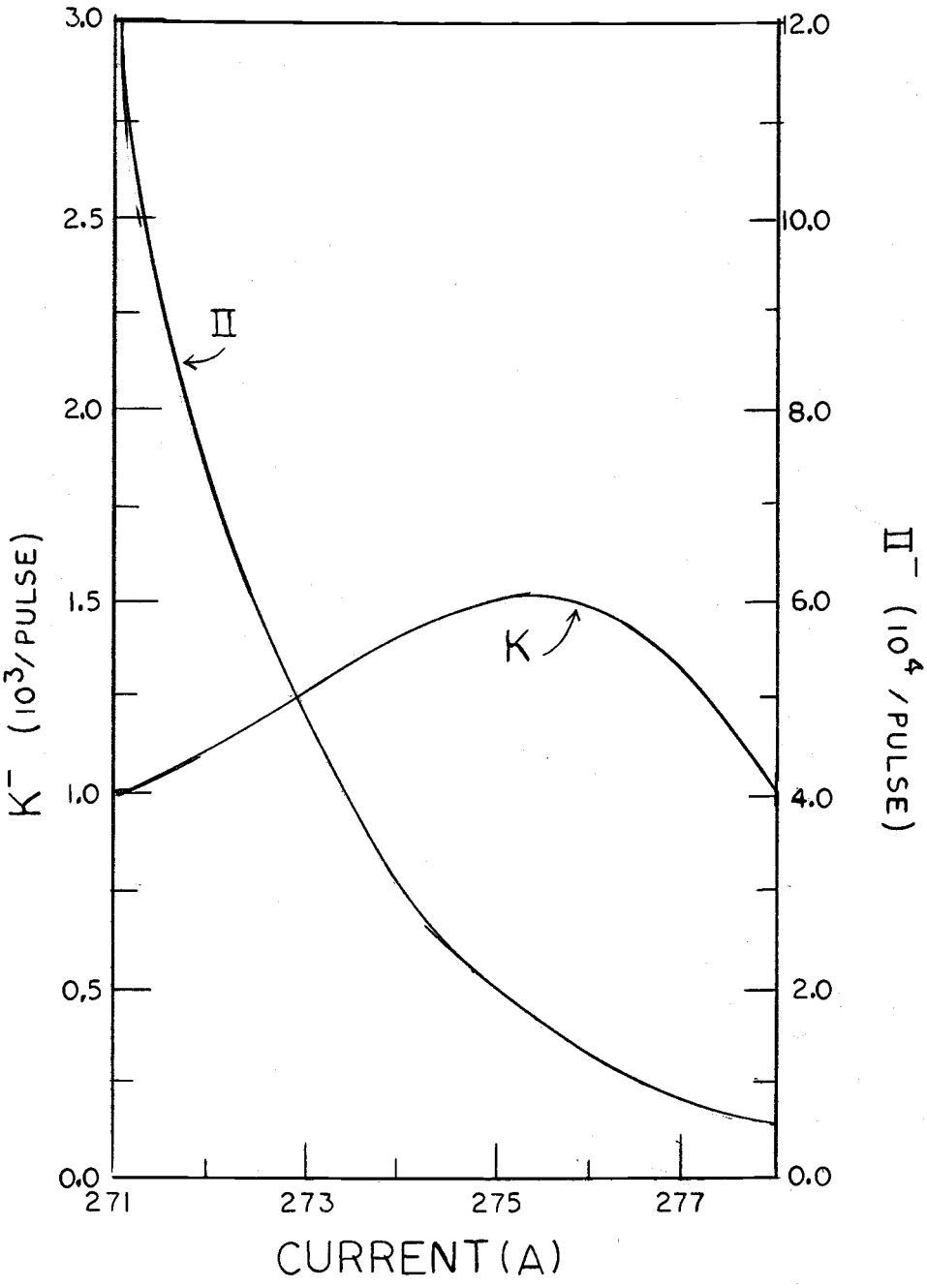

Figure 23. Spectrometer magnet curve.

The flux of kaons was found to be a maximum for a Bevatron energy of 5.9 GeV at spill time and with the internal target positioned at a radius of 599.3" and an azimuthal angle of 79.0 deg. Typical counting rates for certain counters are given in Table 1. During any experiment of this sort there is a constant adjustment of the electronics, the tube voltages, etc. as well as variations in the proton flux striking the internal target. The numbers given represent the average condition during the period of useful data taking. In addition to tending the photomultiplier tubes and electronics, considerable attention was given to the spark chambers so that failures would be quickly spotted. Polaroid snapshots of the operating chambers were taken at regular intervals and underwent immediate examination. At other times there was no shortage of tasks, as is evidenced by the checklist shown in Table 2. In spite of power failures, liquid hydrogen leaks, and broken counters, the experiment was run without serious interruption during the allocated time periods. A discussion of the data obtained and how it was handled will be presented in the following chapters.

Table 1. Typical counting rates.

Protons incident on the internal target	3×10^{12} per pulse
SBEAM	20,000
BEAM	3,050
ABEAM	3,000
NBEAM	40
GOOD EVENT	1.5

Table 2. Checklist.

1. Spectrometer magnet setting
2. Helium bag supply
3. Liquid hydrogen dewar
4. Liquid hydrogen reservoir
5. Liquid hydrogen flask
6. Cerenkov counter nitrogen bottle
7. Cerenkov counter pressure
8. Recirculating carts
9. Neon bottle
10. Helium bottle
11. Spark chambers and cameras
12. Spark gaps - nitrogen bottle
13. Spark chamber power supplies

DATA REDUCTION

During the experiment about 800,000 pictures were taken, of which some 200,000 were obtained while running with the kaon beam. Of these 200,000 pictures, which resided on about 1600 rolls of film, it was known that only a very small percentage could have resulted from the reaction of interest. Fom the known flux incident on the hydrogen target, one would expect only about 1000 events (Appendix I). The spurious triggers resulted from a combination of backround reactions with the

1) inefficiency of counter T3;
2) finite size of T3;
3) photomultiplier signals due to neutrons from the accelerator;
4) photomultiplier tube noise; and
5) malfunctioning of electronics and tube bases.

There may have been other sources of backround, but the above list certainly includes the most important. This chapter is concerned with data reduction: the manner in which the first stage of true event selection was carried out and how the data were recorded on magnetic tape for further study by means of the computer.

A true event is now defined to be a collection of tracks resulting from the reaction of interest. A good event, as discussed previously, was any circumstance leading to the triggering of the spark chambers.

The first step in culling out the true events was a visual scanning of each photograph to find candidates. The main criterion was that there be a single incoming track and four outgoing tracks. In addition, the four tracks must have conceivably resulted from the decays of a k^0 and a Λ. That is to say, each pair of projected tracks must have formed a "V" characteristic of a neutral particle decay. A typical 2V topology is shown in Figure 24. The scanners registered the frame and roll numbers of each candidate along with pertinent details about the picture. Pictures in which one or two seemingly independent particles were seen in the spark chambers were also noted for informational purposes. Pictures with "straight-through" or "stray" particles were not considered candidates, but certainly represented a significant part of the data. It is estimated that one-half of the true events were lost by ignoring such pictures. Unfortunately the time, expense, and added complexity involved in analyzing these pictures prohibited their inclusion. A fraction of the film was looked at a second time to give an estimate of the efficiency for finding candidates. This scanning efficiency turned out to be 95%.

The 2V pictures selected by the scanners were next measured on the SCAMP measuring system. By means of this system the coordinates of all sparks and fiducials were registered on magnetic tape. Details about the SCAMP system are in Appendix II. The measuring procedure involved a second stage of scanning since the

Figure 24. Typical 2V topology.

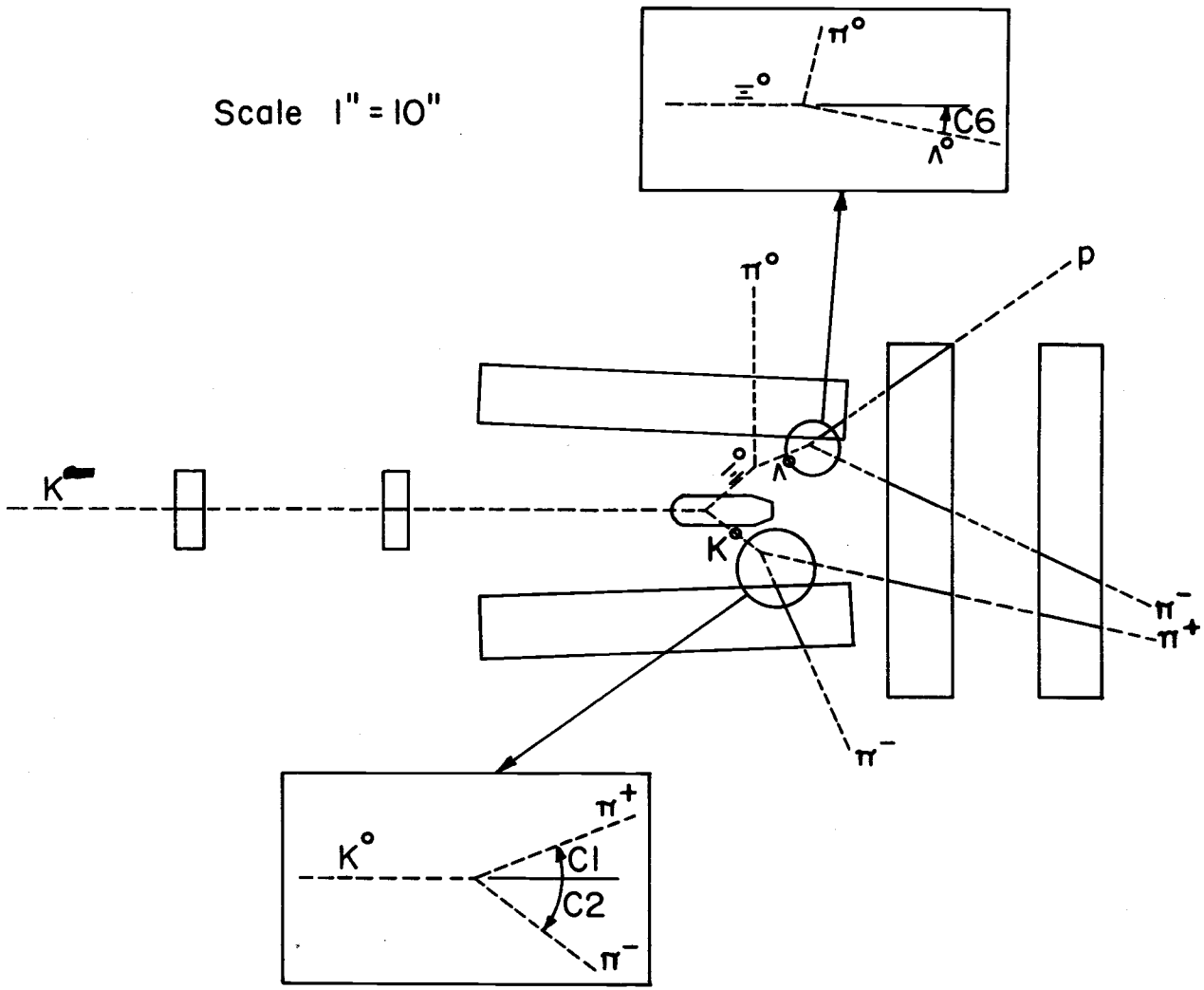
Scale 1" = 10"
π°
Ξ°
C6
Λ°
π°
p
K⁻
Ξ°
Λ°
K°
π⁻
π+
π⁻
π+
K°
C1
C2
π⁻

measurers could discard unsatisfactory pictures. Such pictures included those in which no correlation could be made between the top and side views of a track as well as those in which the scanners had apparently overlooked a disqualifying feature. It turned out that about 99% of the scanning candidates were actually measured. When the measuring was completed in June 1969, the data was contained on 15 reels of magnetic tape.

The final steps in the reduction of the data were handled by the computer, which was used to reconstruct the measured tracks in real space. The reconstruction program first checked the format of the SCAMP data to verify that all fiducials and both views of five tracks had been measured completely and in the proper sequence. After a little more editing the data were stored in arrays and processed in the manner described in Appendix III. Program GEOMET successfully reconstructed 90% of the pictures and the track parameters then resided on 15 geometry tapes. The next step, described in Chapter X, was to analyze these events on the basis of their kinematics in a further effort to isolate the true events.

DATA ANALYSIS

The output of the geometry program consisted of the track directions for some 4500 pictures. Now each picture contained four outgoing tracks which could be grouped together in six different ways. Since there was no way of knowing the proper pairings, each configuration had to be treated as a potential true event. Naturally, choices had to be made eventually so that no more than one event in the final sample came from a single picture.

Analysis of the events on the geometry tapes began with program RECON which employed an iterative process in fitting certain aspects of an event to a given hypothesis. The techniques involved were derived from the methods used in analyzing bubble chamber data (8, 59, 60) and are described in more detail in (39). For those iterations which converged, a chi-squared value was obtained for the final answer. This measure of the "goodness of the fit" was later used to decide which events to accept and which to reject. Table 3 gives those RECON output values which entered into the differential cross section determination.

The quantities CHK and CHL came from two "vertex" fits in which each pair of tracks were hypothesized to have originated at a common vertex; the k^0 or Λ decay point. After a successful vertex fit it was possible to determine the missing mass associated

Table 3. Reconstruction program output.

PB - beam momentum (MeV/c)

CKL - cosine of the k^0 production angle with respect to the beam direction

RI(1) - x value of Ξ^0 production point (inches)

RI(2) - y value of Ξ^0 production point

RI(3) - z value of Ξ^0 production point

Z - perpendicular distance of production point from beam direction (inches)

SK - distance travelled by the k^0 before decay

ESK - error in SK

PK - k^0 momentum

RK - k^0 decay point (see (RI)

CHK - χ^2 for the k^0 vertex fit

CHL - χ^2 for the Λ vertex fit

CHC - χ^2 for the fit to the cascade hypothesis

RM - missing mass associated with the k^0

CHI - the largest χ^2 obtained during the least squares fitting of the sparks

with the neutral particle which was presumed to have decayed at that vertex (Figure 25). The decision as to which vertex belonged to the k^0 was deferred until later; at this point each configuration was still treated as a separate event.

The remaining quantities in Table 3 were determined by an overall fit of the event to the hypothesis that it was indeed an example of

$$k^- + p \rightarrow k^0 + \Xi^0$$

with

$$k^0 \rightarrow \pi^+ + \pi^-.$$

This fit varied the track parameters and k^- momentum to insure that the missing mass associated with the k^0 was that of the neutral cascade. If there was convergence for both vertices in this two-constraint fit, the choice as to which belonged to the k^0 could have been made on the basis of CHC. It turned out, however, that one or the other of the alternatives was always eliminated by the later cuts so that a prior choice was not necessary.

Having determined the laboratory quantities PB and CKL, relativistic kinematics yielded the center of mass quantity CKCM. This and other related calculations are shown in Appendix IV. At this point there was still considerable contamination of the data by backround events so that further cuts were necessary to obtain a

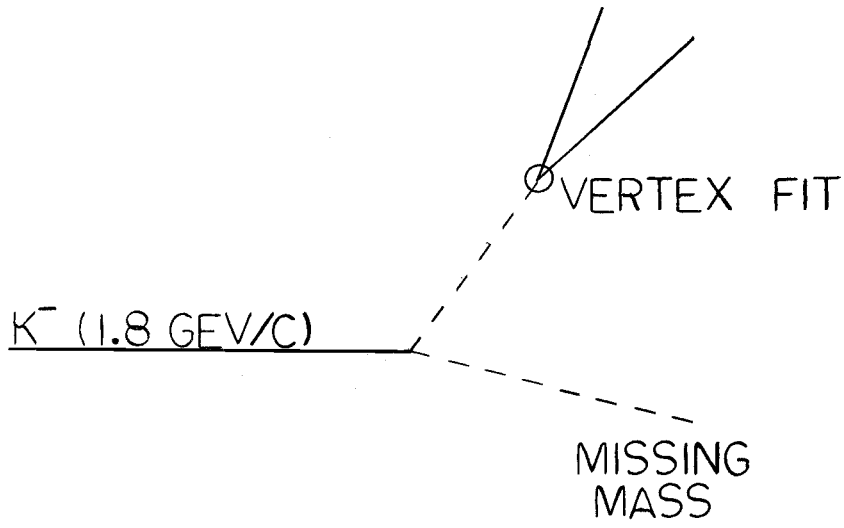

Figure 25. Missing mass determination.

relatively undistorted picture of the differential cross section. The philosophy behind the decisions as to which cuts to make involved several considerations:

1) the cuts should, a priori, eliminate significantly more background than true events;
2) the differential cross section should not be biased; and
3) derived quantities such as the k^0 lifetime should be close to their known values.

The cuts that were made and the number of events which survived are given in Table 4. Number one put a limit on the chi-squared value for the least-square fitting of the sparks. Number two essentially insured that the event was of the 2V variety. The third cut required the missing mass to be near that of the neutral cascade, while four and five eliminated those events in which the production point was outside the liquid hydrogen flask. Finally, cuts six and seven put limits on the natural lifetime of the k^0. By requiring TAU to exceed 0.2 inches, one would hope to avoid instances whereby the charged particles emerged from the production vertex rather than from a decay vertex. The other limitation on TAU was meant to cut out a few especially long lived k^0's which one would not expect to observe on the basis of the known lifetime. The resulting final sample consisted of 59 events which implied a total cross section consistent with previous results (Figure 26). Some

Table 4. Effect of cuts on the number of events.

	Restrictions on the data	Number of events passing
	$1.1 < RM < 1.5$ GeV/c^{2*}	274
1	$CHI \leq 100$	260
2	$CHK,\ CHL < 6$	235
3	$1.2 < RM < 1.4$	120
4	$-26. \leq RI(1) \leq -20.$	213
5	$Z \leq 1$	253
6	$TAU > 0.2$	200
7	$TAU < 4.0$	266

*Made within program RECON.

FLUX DETERMINATION

Total flux during the experiment: 7.5×10^{7} k^{-}.

Multiply this by

0.50 for unmeasured pictures (stray, straight-thrus)

0.90 for deadtime in the anticoincidence counter

0.90 for events lost by measuring errors, then

the total corrected flux = 3.0×10^{7} k^{-}.

YIELD DETERMINATION

Number of events in final sample: 59

Multiply this by

5.5 for branching ratios

4.0 for the detection efficiency

1.5 for the reconstruction efficiency, then

the total corrected number of events = 1900.

One has

$1900 = 3.0 \times 10^{7} (\sigma \cdot 66 \times 10^{22})$ (see appendix I)

$\sigma = 9.6 \times 10^{-29}$

$\sigma = 96$ microbarns.

Unfortunately, the flux determination is only an estimate because not all of the film was measured. Thus, this total cross section can really only be used as a consistency check. A recent determination (25) of the cross section yielded the value 100 ± 23 microbarns.

Figure 26. Derivation of the total cross section.

distributions of interest are the production point, missing mass, and k^0 lifetime. These are displayed in Figure 27. The CKCM distribution is not the differential cross section, since no correction has yet been made for the experimental detection efficiency as a function of CKCM. The way in which Monte Carlo methods were used to make this correction is the subject of the next chapter.

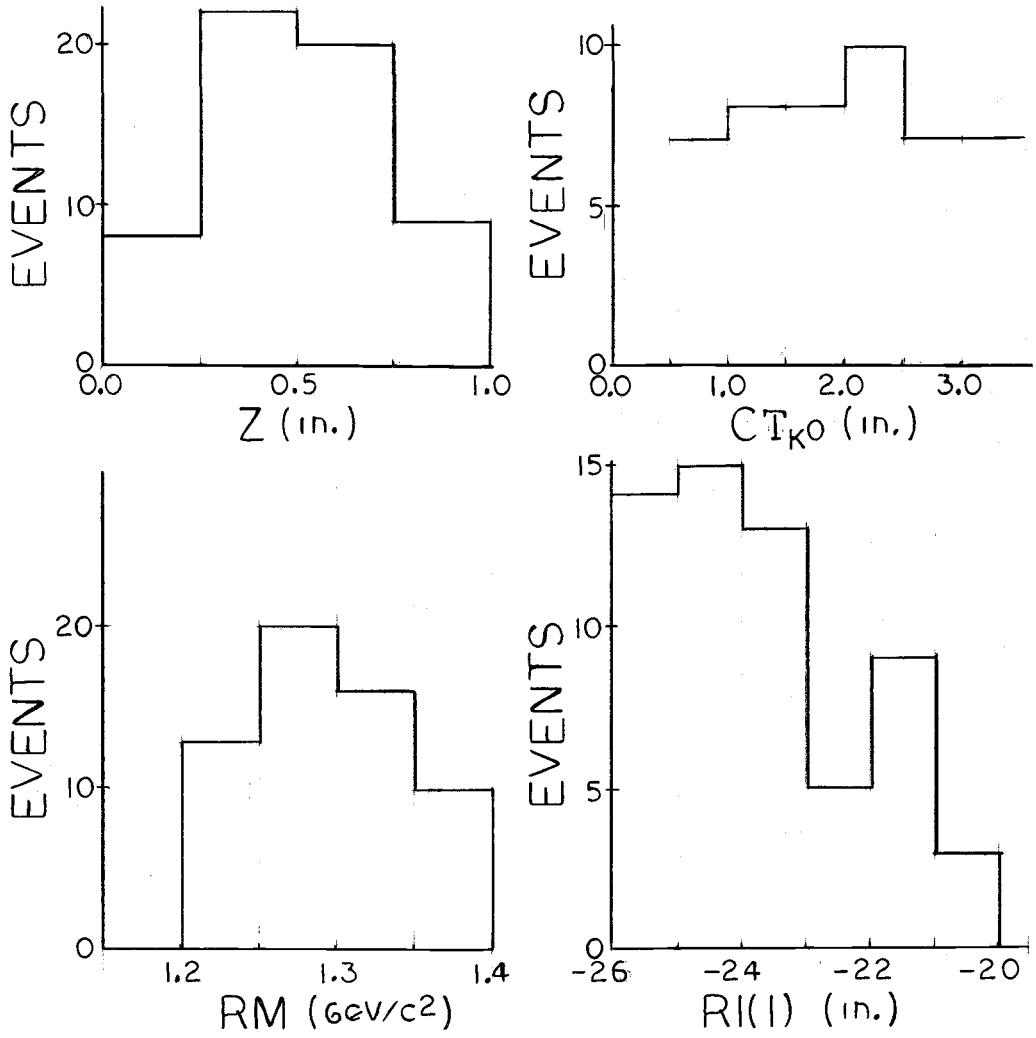

Figure 27. Experimental distributions.

MONTE CARLO CORRECTION

In most spark chamber experiments the counters used to identify the reaction of interest do not completely surround the target, and so a certain fraction of the true events are lost. If this effect tends to deplete the bins of certain center of mass production angles, then a correction must be made to obtain the true differential cross section. The availability of high speed computers has made the Monte Carlo method the most convenient and accurate means for making such a geometrical correction. The mathematical basis for the Monte Carlo method may be found in (76). In this chapter only those aspects which apply to the experiment at hand will be covered.

As they apply to this experiment, the Monte Carlo calculations involved the following steps:

1) a mathematical model of the experiment was set up;
2) a set of center of mass production angles (events) was generated;
3) each event was assigned other kinematic values on the basis of known distributions;
4) the events were examined to see if they would have been detected and subsequently reconstructed; and
5) the distribution of reconstructed events was divided by the distribution of generated events to obtain the detection efficiency

as a function of the center of mass production angle. Then dividing the experimental distribution by the detection efficiency yielded the true differential cross section. Figure 28 shows the two Monte Carlo distributions used to obtain the detection efficiency. Details about the calculations are presented in Appendix V.

Besides providing a correction factor, the Monte Carlo results can also be used to check other experimental distributions. Figure 29 shows the theoretical distribution of production points along the x axis. The similarity of this plot with the experimental one in Figure 27 makes one more confident that the anti-coincidence counter was working properly and also that there was not a large number of interactions in the counter just in front of the target. Also, the experimental missing mass distribution for the final events is certainly consistent with the Monte Carlo prediction. These results, then, tend to reinforce the view that the differential cross section, presented in the next chapter, is based on an essentially unbiased sample of true events.

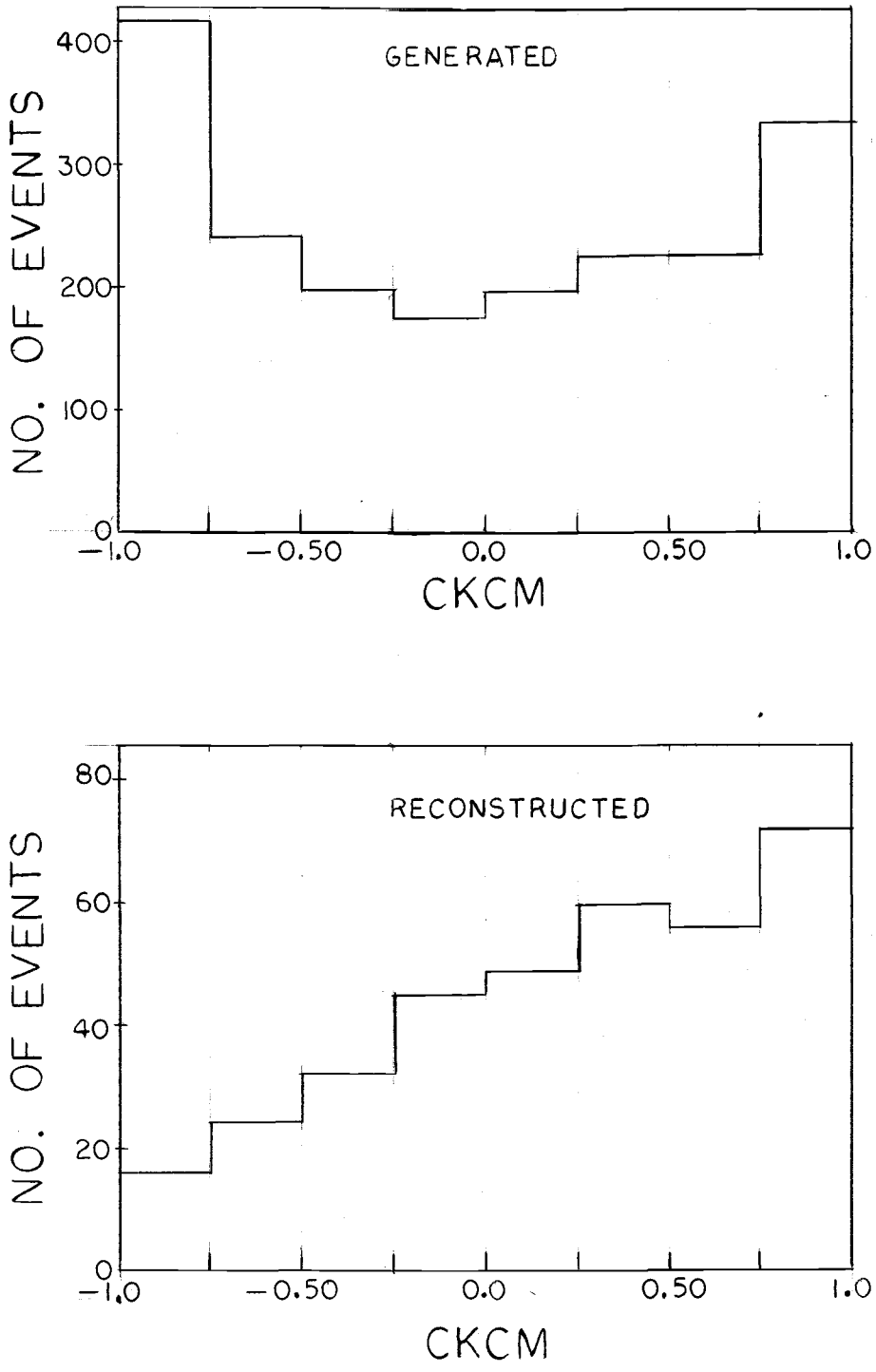

Figure 28. Detection efficiency determination.

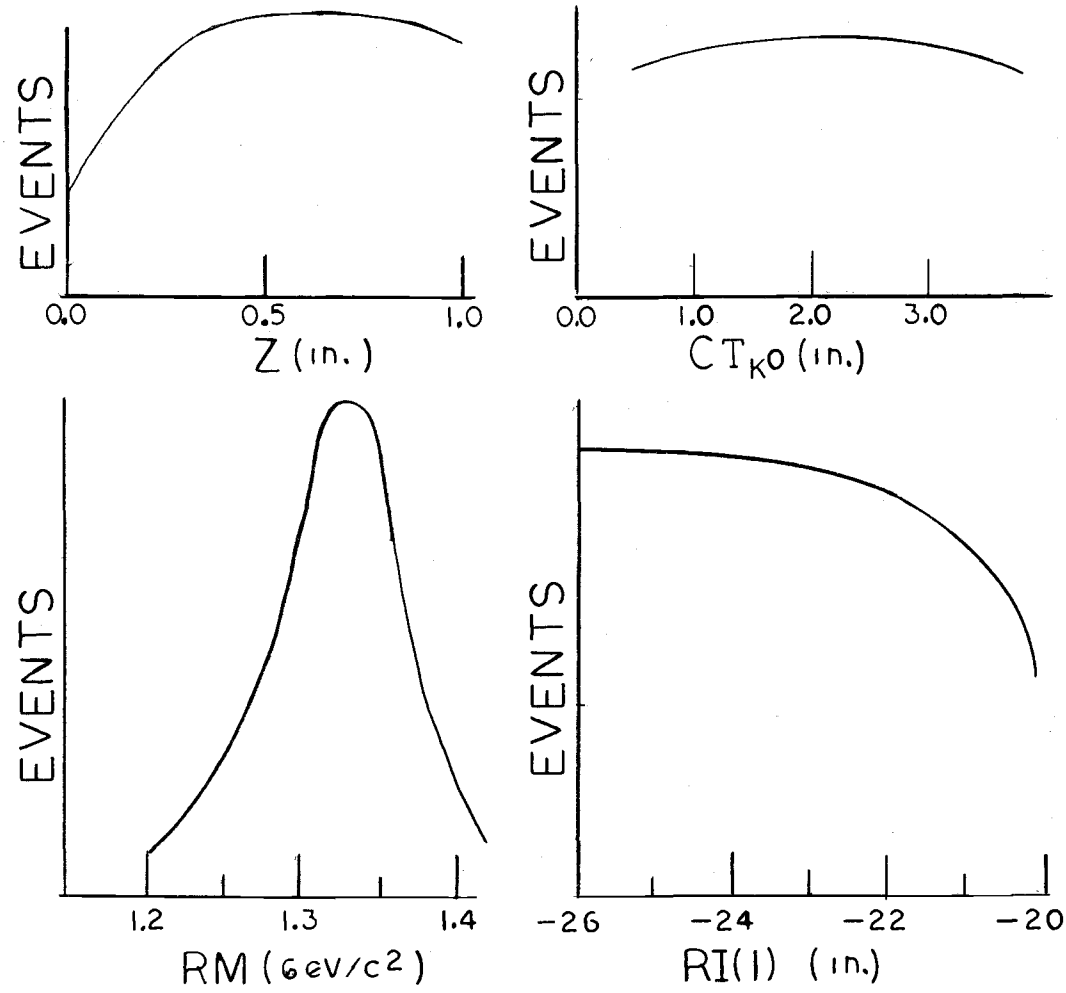

Figure 29. Theoretical distributions.

DIFFERENTIAL CROSS SECTION

To get an analytical expression for the differential cross section, the 59 values of CKCM were first distributed among eight bins. The number of events in each bin was divided by the appropriate detection efficiency, the resulting populations renormalized, and then fit to a series of Legendre polynomials. The advantages resulting from using Legendre polynomials are well known; their orthogonality allows the addition of further terms without greatly affecting the lower ones, and the coefficients are rather easily related to the amplitudes entering into a partial wave analysis. The form of the differential cross section is then

$$\frac{d\sigma}{d\Omega}(CKCM) = \frac{\sigma}{4\pi} \sum_{L=0}^{L = L_{MAX}} \left(\frac{A_L}{A_0}\right) P_L(CKCM)$$

where A_0 is related to the total cross section and the initial state center of mass momentum (25). The coefficients $B_L = A_L/A_0$ do not depend on the normalization and so are useful in comparing the results of different experiments at slightly different momenta. Table 5 gives the coefficients and chi-squared values for fits with different degrees of freedom. The fit is not significantly improved by using more than four polynomials, so that is the number used to plot the final result shown in Figure 30.

Table 5. Legendre polynomial fits.

Degrees of freedom	B0	B1	B2	B3	B4	B5	χ^2
5	1.00±0.30	1.17±0.50	1.00±0.55				7.31
4	1.00±0.27	0.45±0.42	1.08±0.47	-1.20±0.62			3.00
3	1.00±0.32	0.81±0.57	0.56±0.74	-0.99±0.73	-0.83±0.79		1.84
2	1.00±0.33	0.71±0.62	0.64±0.78	-1.18±1.01	-0.81±0.78	-0.27±0.91	1.76

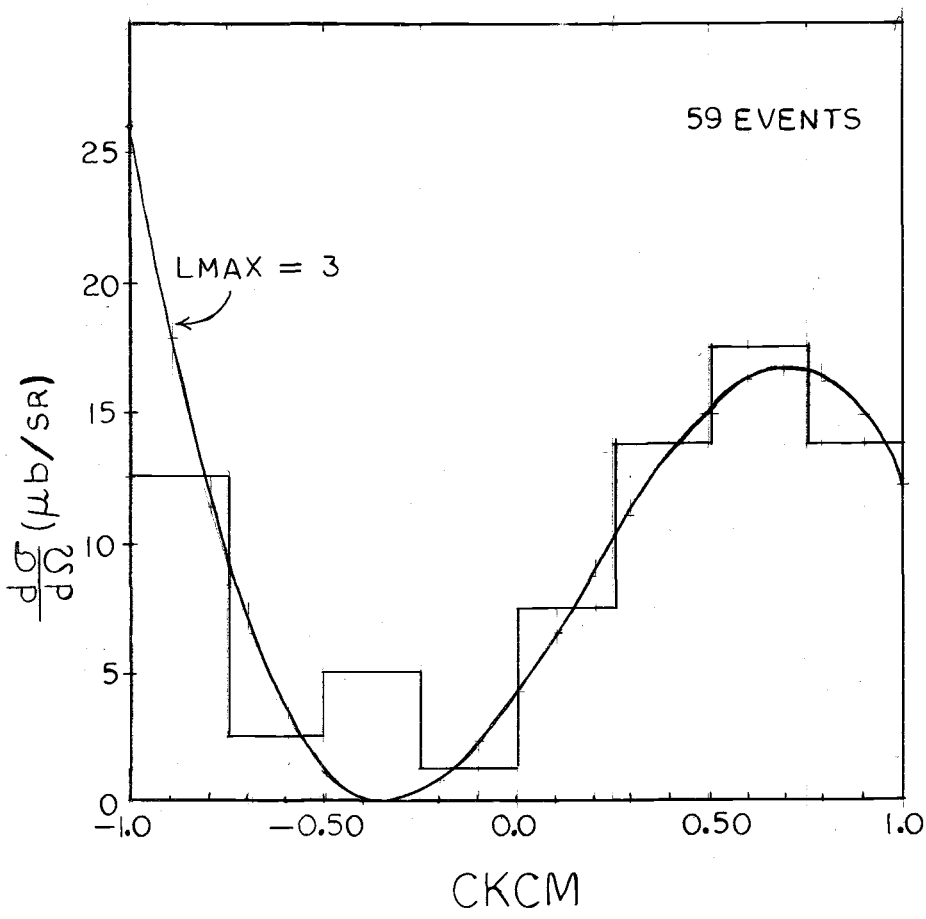

Figure 30. Differential cross section.

The value in measuring this differential cross section lies in the information it can give about the forces which yielded it. According to present theories, there are three different ways in which the nuclear (strong) force can manifest itself:

1) meson exchange (t channel);

2) baryon exchange (u channel); and

3) resonance formation (s channel).

Figure 31 shows the exchange diagrams and the exchange candidates allowed by the conservation laws. Qualitatively, the differential cross section supports the implication of Figure 31 that baryon exchange occurs while meson exchange is absent. The backward (CKCM = -1) peak indicates that a heavy particle is transferring considerable momentum to the k^0. The dip in the forward direction shows the lack of peripherality in the interaction; a sign that there is no long-range meson being exchanged.

At intermediate angles the differential cross section is neither zero nor flat, but shows an undulation characteristic of resonance formation and decay. The known resonances which might be contributing are given in Figure 32. By knowing the spin of the resonance, one can calculate (70) the contribution of its decay to each of the coefficients in the Legendre series. The experimental coefficients are consistent with $\Lambda(2100)$ formation, but clearly are not known accurately enough to rule out other possibilities. In fact,

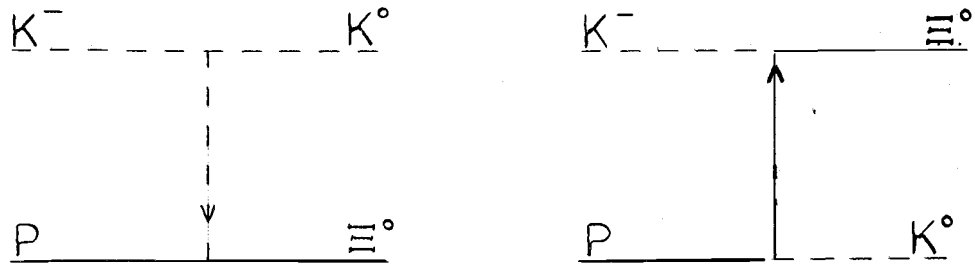

$B = 0$	$B = 1$
$S = 2, -2$	$S = -1$
$Q = 2, -2$	$Q = 1$
$Y = \pm 2$	$Y = 0$
$Q = T_3 + Y/2$	$Q = T_3 + Y/2$
$\pm 2 = T_3 \pm 1$	$1 = T_3 + 0$
$T_3 = \pm 1$	$T_3 = 1$
$T = 1$	$T = 1$
(unknown)	(Σ^+)

Figure 31. Exchange diagrams.

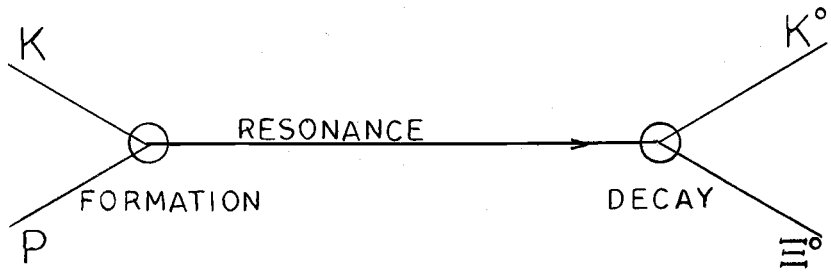

Resonance	I (J^P)
Λ (1815)	0 ($5/2^+$)
Λ (1830)	0 ($5/2^-$)
Λ (2100)	0 ($7/2^-$)
Λ (2350)	0 (?)
Σ (1915)	1 ($5/2^+$)
Σ (2030)	1 ($7/2$)
Σ (2250)	1 (?)

Figure 32. Resonance candidates.

the drawing of any quantitative conclusions would be very difficult without combining the results presented here with those obtained in other experiments. This possibility will be considered in the next chapter.

CONCLUSION

This experiment was not the first to study the reaction

$$k^- + p \rightarrow k^0 + \Xi^0 \quad (1.8 \text{ GeV/c}),$$

but it does represent a significant contribution to the knowledge about the differential cross section. The Saclay (13) and LRL (25) groups base their results on 39 and 50 events, respectively. Qualitatively, both of these results are similar to that obtained in this experiment. Within statistical errors, the LRL coefficients are the same as those reported here. Of course, the errors are large and more events would be very desirable. To carry out a partial wave analysis, more poarization information is required. If such data could be derived from this experiment, a long step could be taken toward pinning down the resonance contributions to the differential cross section. Perhaps the analysis might show the existence of a previously undiscovered enhancement.

Besides a partial wave analysis, one might hope to fit all of the experimental data to a model of the reaction amplitude. If this model were based on SU(3), the $kpk\Xi$ interaction could perhaps be related to other combinations of the members of the basic meson and baryon octets. Lack of knowledge about the Ξ has certainly held up progress in this area, so one hopes that this experiment

will serve as an inducement to elementary particle physicists to extend their theoretical work along these lines.

BIBLIOGRAPHY

1. Ademollo, M. and R. Gatto. Complete spin tests for fermions. The Physical Review 133:B531-B541. 1964.

2. Ademollo, M. and R. Gatto. Methods for determining the spin of Ξ. Nuovo Cimiento (10)30:429-442. 1963.

3. Alvarez, Luis W. et al. Neutral cascade hyperon event. Physical Review Letters 2:215-219. 1959.

4. Alvarez, L. W. et al. Ξ^- hyperons in the reaction $k^- + p \rightarrow \Xi + k^+$. In: Proceedings of the 1962 International Conference on High Energy Physics, CERN, 1962. p. 433-437.

5. Anderson, C. D. et al. Cascade decay of V particles. I. The Physical Review 92:1089. 1953.

6. Armenteros, R. et al. The properties of charged V particles. Philosophical Magazine 43:597-612. 1952.

7. Badier, J. et al. Baryonic states of strangeness -2 produced in k-p interactions at 3.0 GeV/c. Physics Letters 16:171-174. 1965.

8. Berge, J. Peter, Frank T. Solomitz and Horace D. Taft. Kinematical analysis of interaction vertices from bubble chamber data. The Review of Scientific Instruments 32:538-548. 1961.

9. Berge, J. Peter et al. Some properties of Ξ^- and Ξ^0 hyperons produced in k-p interactions between 1.05 and 1.7 BeV/c. The Physical Review 147:945-961. 1966.

10. Bertanza, L. et al. Decay of a negative hyperon into $\Lambda^0 + e^- + \bar{\nu}$. Physical Review Letters 9:19-21. 1962.

11. Bertanza, L. et al. Properties of the Ξ^- hyperon. In: Proceedings of the 1962 International Conference on High Energy Physics, CERN, 1962. p. 437-441. (Physical Review Letters 9:229-232. 1962)

12. Bevatron experimenters handbook. 1969. University of California Lawrence Radiation Laboratory Report UCRL-17333 Rev.

13. Burgun, G. et al. Resonance formation in the reactions $k^- p \rightarrow k^+ \Xi^-$ and $k^- p \rightarrow k^0 \Xi^0$ in the mass region from 1915 to 2168 MeV. Nuclear Physics B8:447-459. 1968.

14. Button-Shafer, Janice et al. Spin and parity of the Ξ^* (1530 MeV). The Physical Review 142:883-887. 1966.

15. Byers, N. and S. Fenster. Determination of spin and decay parameters of fermion states. Physical Review Letters 11: 52-55. 1963.

16. Cabbibo, Nicola. Unitary symmetry and leptonic decays. Physical Review Letters 10:531-533. 1963.

17. Carmony, D. Duane and Gerald M. Pjerrou. Leptonic decay of the Ξ^- hyperon. Physical Review Letters 10:381-384. 1963.

18. Carmony, D. Duane et al. Properties of Ξ hyperons. Physical Review Letters 12:482-485. 1964.

19. Connolly, P. L. et al. Decay characteristics of Ξ^- and Ξ^0 hyperons. In: Proceedings of the Siena International Conference of Elementary Particles, Siena, 1963. p. 34-39.

20. Connolly, P. L. et al. Resonance formation in the $\Xi k \pi$ system. In: Proceedings of the Siena International Conference on Elementary Particles, Siena, 1963. p. 125-129.

21. Crawford, F. S. et al. Detection of parity nonconservation in Λ decay. The Physical Review 108:1102-1104. 1957.

22. Crawford, Jr., F. S. Strange-particle decays. In: Proceedings of the International School of Physics "Enrico Fermi" Course XXVI. New York, Academic Press, 1963. p. 88-148.

23. Crawford, F. S. Weak interactions of strange particles. In: Proceedings of the 1962 International Conference on High Energy Physics, CERN, 1962. p. 827-831.

24. Cronin, James W. and Oliver E. Overseth. Measurement of the decay parameters of the Λ^0 particle. The Physical Review 129:1795-1807. 1963.

25. Dauber, Phillip M. et al. Production and decay of cascade hyperons. The Physical Review 179:1262-1285. 1969.

26. Eberhard, Phillipe, Janice Button-Shafer, and Deane W. Merrill. Decay properties of the Ξ^- hyperon. 1964. 7 p. University of California Lawrence Radiation Laboratory Report UCRL-11427.

27. Eisler, F. et al. Demonstration of parity nonconservation in hyperon decay. The Physical Review 108:1353-1355. 1957.

28. Ferro-Luzzi, Massimiliano et al. Upper limit for the nonleptonic $\Delta S = 2$ decay mode of Ξ^-. The Physical Review 130: 1568-1570. 1963.

29. Fowler, William B. et al. Ξ^- production by k^- mesons. Physical Review Letters 6:134-136. 1961.

30. Frazer, William R. Elementary particles. Englewood Cliffs, Prentice-Hall, 1966. 190 p.

31. Gasiorowicz, Stephan. Elementary particle physics. New York, John Wiley and Sons, 1966. 613 p.

32. Gatto, R. and H. P. Stapp. Spin and parity analysis from production and decay of hyperon resonant states. The Physical Review 121:1553-1555. 1961.

33. Gell-Mann, Murray. Nonleptonic weak decays and the eightfold way. Physical Review Letters 12:155-156. 1964.

34. Gell-Mann, M. California Institute of Technology Report CTSL-20. 1961.

35. Gell-Mann, M. and A. Pais. Theoretical views on the new particles. In: Proceedings of the International Conference on Nuclear and Meson Physics, Glasgow, 1954. p. 342-352.

36. Halsteinslid, A. et al. Preliminary results on $\Xi^- + k^\pm + n\pi$ final states produced by 3.5 GeV k^-. In: Proceedings of the Siena International Conference on Elementary Particles, Siena, 1963. p. 173-178.

37. Hubbard, John Richard. Properties of the neutral cascade hyperon. 1966. 55 p. University of California Lawrence Radiation Laboratory Report UCRL-11510.

38. Hubbard, J. Richard et al. Lifetimes of the Ξ^- and Ξ^0 hyperons. The Physical Review 135:B183-B187. 1964.

39. Jauch, D. E. Measurement of the neutral cascade hyperon lifetime. Doctoral dissertation. Corvallis, Oregon State University (to be published).

40. Jauneau, L. et al. Ξ^0 properties. In: Proceedings of the Siena International Conference on Elementary Particles, Siena, 1963. p. 1-4.

41. Jauneau, L. et al. Ξ^- properties. In: Proceedings of the Siena International Conference on Elementary Particles, Siena, 1963. p. 4-7. (Physics Letters 5:261-265. 1963)

42. Jauneau, L. et al. Direct measurement of Ξ^- and Ξ^0 mean lives. Physics Letters 4:49-51. 1963.

43. Jelley, J. V. Cerenkov radiation and its applications. New York, Pergamon Press, 1958. 304 p.

44. Källen, Gunnar. Elementary particle physics. Reading, Addison-Wesley, 1964. 546 p.

45. Koch, W. Determination of the Ξ decay parameters. In: Proceedings of the 1964 Easter School for Physicists. Vol. 2. CERN 64-13 Geneva, 1964. p. 75-111.

46. Kokkedee, J. J. J. The quark model. New York, W. A. Benjamin, 1969. 239 p.

47. Lawrence Radiation Laboratory counting handbook. 1964. University of California Lawrence Radiation Laboratory Report UCRL-3307 Rev. 2.

48. Lee, Benjamin W. Transformation properties of nonleptonic weak interactions. Physical Reveiw Letters 12:83-86. 1964.

49. Lee, T. D. and C. N. Yang. Elementary particles and weak interactions. 1957. 61 p. Brookhaven National Laboratory Report BNL 443 (5-91).

50. Lee, T. D. and C. N. Yang. Possible determination of the spin of Λ^0 from its large decay angular asymmetry. The Physical Review 109:1755-1758. 1958.

51. Lee, T. D. and C. N. Yang. Question of parity conservation in weak interactions. The Physical Review 104:254-258. 1956.

52. Lee, T. D. et al. Possible detection of parity nonconversation in hyperon decay. The Physical Review 106:1367-1369. 1957.

53. Lipkin, H. J. Unitary symmetry for pedestrians. 1964. 32 p. Argonne National Laboratory Report ANL-6942.

54. London, G. W. et al. K^--p interactions at 2.24 BeV/c. The Physical Review 143:1034-1091. 1966.

55. Merrill, Jr., Deane Whitney. Decay properties of the Ξ^* resonances. 1966. 183 p. University of California Lawrence Radiation Laboratory Report UCRL-16455.

56. Ne'eman, Y. Nuclear Physics 26:222- . 1961.

57. Orear, Jay. Notes on statistics for physicists. 1958. 34 p. University of California Lawrence Radiation Laboratory Report UCRL-8417.

58. Pjerrou, G. M. et al. Resonance in the ($\Xi\pi$) system. at 1.53 GeV. Physical Review Letters 9:114-117. 1962.

59. Ronne, B. Kinematical analysis of bubble chamber pictures. In: Proceedings of the 1964 Easter School for Physicists. Vol. 1. CERN 64-13 Geneva, 1964.

60. Rosenfeld, Arthur H. and James N. Snyder. Digital-Computer analysis of data from bubble chambers; kinematic analysis of complete events. The Review of Scientific Instruments 33: 181-195. 1962.

61. Rosenfeld, Arthur H. et al. Data on particles and resonant states. Reviews of Modern Physics 40:77-128. 1968.

62. Rossi, Bruno. High energy particles. Englewood Cliffs, Prentice-Hall, 1952. 569 p.

63. Sakurai, J. J. Invariance principles and elementary particles. Princeton, Princeton University Press, 1964. 326 p.

64. Samios, N. P. Hyperon non-leptonic decays. In: Proceedings of the International Conference on Weak Interactions, Argonne, 1965. p. 189-202.

65. Schlein, P. E. et al. Spin-parity determination of the $\Xi\pi$ resonance (1.530 GeV). Physical Review Letters 11:167-171. 1963.

66. Schneider, H. Mass and decay parameters of Ξ-particles. Physics Letters 4:360-361. 1963.

67. Smith, Gerald A. et al. Production and decay of Ξ^{*} (1820). Physical Review Letters 14:25-28. 1965.

68. Smith, Gerald A. et al. Study of $S = -2$ baryon systems up to 2 BeV. Physical Review Letters 13:61-66. 1964.

69. Sossong, Norman Dale. An experimental study of $k^{-}p$ charge exchange at 1.8 BeV/c. Doctoral dissertation. Seattle, University of Washington, 1969. 139 numb. leaves (microfilm)

70. Stevenson, M. L. et al. New experimental test of the decay rate prediction, $2\,\Xi^{-} \rightarrow \Lambda_{-} + \sqrt{3}\,\Sigma_{0}^{+}$. Physical Letters 9:349-351. 1964.

71. Sugawara, Hirotaka. A new triangle relation for non-leptonic hyperon decay amplitudes as a consequence of the octet spurion and the R symmetry. Progress of Theoretical Physics 31: 213-221. 1964.

72. Teutsch, W. B., S. Okubo, and E. C. G. Sudarshan. Decay of cascade particles. The Physical Review 114:1148-1149. 1959.

73. Ticho, Harold K. The present status of Ξ decay. In: Proceedings of the Conference on the Fundamental Aspects of Weak Interactions, Brookhaven National Laboratory, 1963. p. 410-421.

74. Tripp, Robert D. Baryon resonances. CERN 65-7 (Rev.) Geneva, 1965. 54 p.

75. Trippe, Thomas G. and Peter E. Schlein. Partial-wave analysis of $k^- p \rightarrow \Xi^- k^+$ at 2 GeV/c. The Physical Review 158: 1334-1337. 1967.

76. Werbrouck, A. Notes on the Monte Carlo method. In: Proceedings of the 1964 Easter School for Physicists. Vol. 1. CERN 64-13 Geneva, 1964. p. 147-176.

APPENDICES

YIELD OF THE HYDROGEN TARGET

Since the total k^--p cross section is small, the beam is attenuated only slightly by the target. In this case the flask may be treated as a thin disk and the probability of a reaction is just the area of the scattering centers divided by the cross sectional area of the flask:

$$P = \sigma \cdot (\text{number of scattering centers/cm}^2)$$

$$= \sigma N_O \rho \, l/A.$$

Putting in the numbers,

$$P = (100 \times 10^{-30} \text{ cm}^2)(6 \times 10^{23} \text{ atoms/mole}).$$

$$(6 \times 2.54 \text{ cm})/1 \text{ gm/mole}$$

$$= 66 \times 10^{-6}.$$

The total flux on the target was about 10^8 kaons, so the number of neutral cascades produced was on the order of 6000. This is, of course, an upper limit because of branching ratios and the finite detection efficiency. Later on the total cross section will be derived from the numbers obtained in this experiment.

SCAMP SYSTEM

The SCAMP measuring system of the Lawrence Radiation Laboratory is a semi-automatic measuring machine consisting of a film transport system, a projection apparatus, a panel of switches, and a tape recording mechanism. The SCAMP is film-plane digitized with the smallest increment on the film being one micron.

In handling an event, the measurer would place the crosshair on each fiducial mark and then on every visible spark, all in a prescribed order. Depressing a foot pedal registered the coordinates of the crosshair within the machine. At this stage mistakes could still be rectified by pushing an "error" button on the panel. After 20 measurements had been made, the accumulated data was recorded on tape by pushing yet another button. In addition to the measured points, the panel information was also recorded. The binary and decimal switches on the panel were used to convey such information as roll number, frame number, scanner number, and date.

Several different groups are able to use the SCAMP by each inserting their own patchboard containing their particular format. The data is then distinguished by a format number and each week computer center personnel copy appropriate records from the master tape onto each group's individual tape. These were called SCAMP tapes and were the input to the geometry program.

GEOMETRY PROGRAM

To reconstruct the spark chamber tracks, a coordinate system was set up within the experimental house. One fiducial mark was taken to be the origin and all others were surveyed to determine their coordinates. A righthanded system was employed, with positive x along the nominal beam line and positive z along the vertical.

The cameras viewed the spark chambers through a system of mirrors whose positions were also surveyed. By using geometry, the optical paths were unfolded to determine the position of "virtual" cameras. A virtual camera was located at a point in space where it had a direct view identical to that reflected by mirrors into the corresponding real camera. The virtual cameras, then, replaced the real cameras and there was no longer any need to consider the mirrors.

The SCAMP measuring system supplied the film coordinates (x_F, y_F) of the sparks and fiducials. The survey yielded the space coordinates (x_S, y_S, z_S) of the fiducials and it was desired to find the space coordinates of the sparks. In each view of every spark chamber there were placed three or four fiducials in a plane. This fiducial plane was designed to be parallel to the virtual film plane so that a transformation of the form

$$x' = Ax_F + By_F$$

$$y' = Cx_F + Dy_F$$

could be set up. The known fiducial coordinates were used to determine the constants, and then the fiducial plane coordinates of each spark were determined. In principle, only two fiducials per view were required, but the excess allowed the constants to be determined by a least-squares fitting.

To find the positions of the sparks in space, the two views of each chamber had to be correlated in the following manner. The spark positions in a top fiducial plane (Z1, Z2, Z3, Z4 in Figure 33) were fit to a straight line by the method of least squares. The "track" plane defined by this line and the top virtual camera was then known to contain the actual track.

The line joining the side virtual camera to the side fiducial plane spark positions (Z5, Z6, Z7, Z8) was intersected with the track plane to give the space coordinates of the sparks (Z9, Z10, Z11, Z12). Finally, the true spark coordinates were fit by least squares on the track plane to give the track direction. For fitting purposes the tracks were parameterized by projecting them onto the X-Z and Y-Z planes. Thus the geometry program supplied five track directions in the form

$$x = az + b$$

$$y = cz + d.$$

Included were the errors which were propagated to give the uncertainty in kinematic quantities.

Figure 33. Reconstruction diagram.

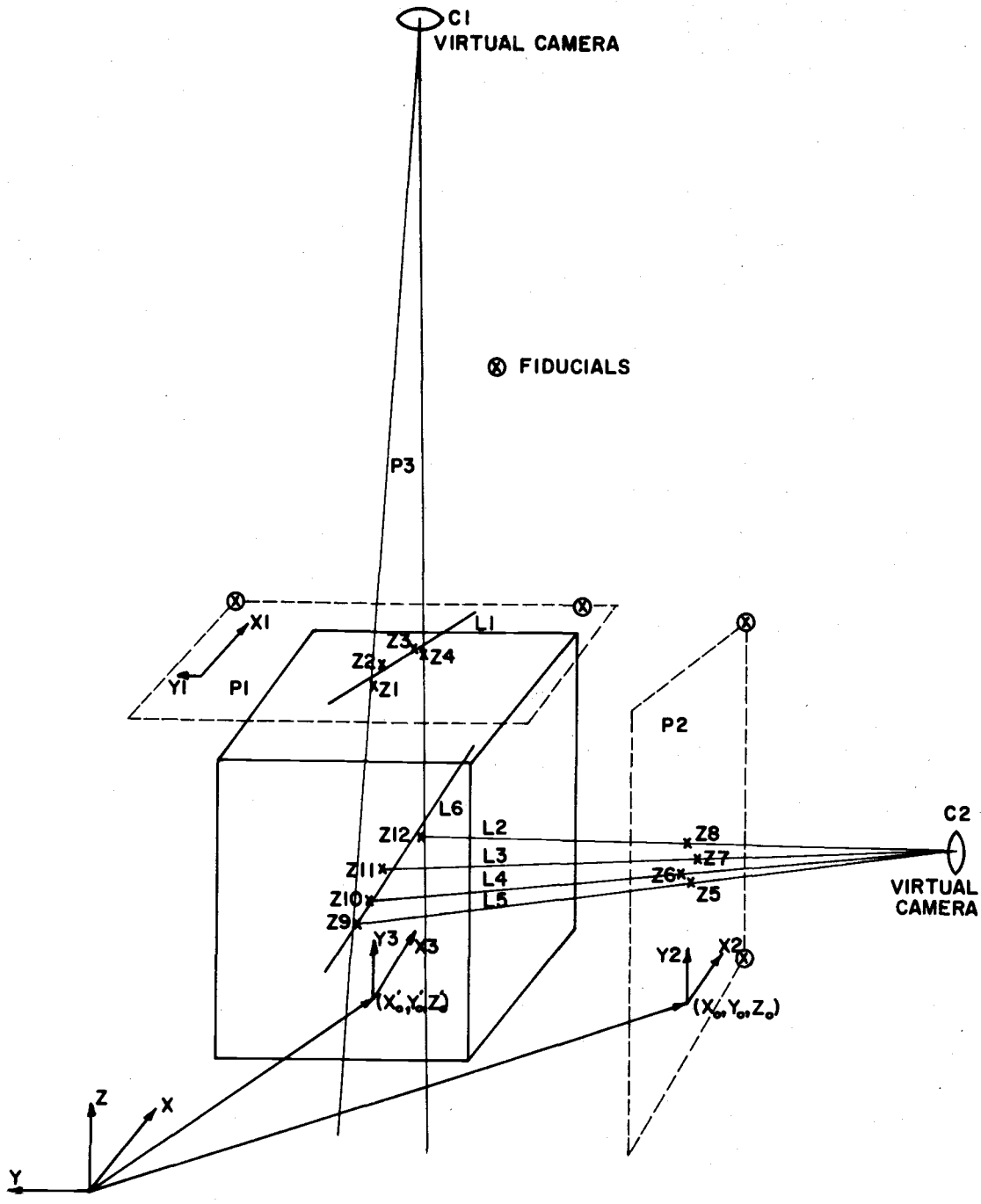
C1
VIRTUAL CAMERA
⊗ FIDUCIALS
P3
X1
Y1
P1
L1
Z3
Z2
Z4
Z1
P2
L6
L2
L3
L4
L5
Z12
Z11
Z10
Z9
Z8
Z7
Z6
Z5
C2
VIRTUAL CAMERA
Y3
X3
(X'o,Y'o,Z')
Y2
X2
(Xo,Yo,Zo)
Z
X
Y

RELATIVISTIC KINEMATICS

For a reaction $1 + 2 \rightarrow 3 + 4$, one generally starts with the knowledge or assumption of the beam momentum p_1. In this case the center of mass quantities may be determined in the following manner. Letting a prime denote a center of mass quantity and a bar indicate a four-vector, one has

$$\begin{aligned} &= (\underline{p}_1 + \underline{p}_2)^2 \\ &= [(E_1 + M_2), \bar{p}_1]^2 \\ &= E_1^2 + 2E_1M_2 + M_2^2 - p_1^2 \\ &= m_1^2 + M_2^2 + 2E_1M_2, \text{ and} \\ E' &= \sqrt{s}. \end{aligned}$$

Then for the center of mass,

$$\beta = p_1/(E_1 + M_2)$$

$$\gamma = (E_1 + M_2))/E' .$$

Now if one has assumed the beam momentum and has measured the emission angle and momentum (by the decay opening angle) of particle 3, then the missing mass may be found by four-vector conservation:

$$\underline{p}_1 + \underline{p}_2 = \underline{p}_3 + \underline{p}_4$$

$$\underline{p}_4 = \underline{p}_1 + \underline{p}_2 - \underline{p}_3$$

$$MM = (\underline{p}_4)^2 = (\underline{p}_1 + \underline{p}_2)^2 - 2(\underline{p}_1 + \underline{p}_2)\cdot\underline{p}_3 + \underline{p}_3^2$$

$$= s - 2\underline{p}_1\cdot\underline{p}_3 - 2\underline{p}_2\cdot\underline{p}_3 + m_3^2$$

$$= s - 2E_1E_3 + 2p_1p_3\cos\theta - 2M_2E_3 + m_3^2.$$

If, instead, the fitting program has yielded the beam momentum and the emission angle θ, the center of mass angle may be found by using a Lorentz transformation:

$$p_3'\cos\theta' = \gamma(p_3\cos - \beta E_3)$$

and the conservation laws

$$p_3' = p_4'$$

$$E_3' + E_4' = E'.$$

The mass values used in these calculations are given in Table 6.

Table 6. Elementary particle masses.

Particle	Mass (MeV/c^2)
K^-	493.830
P	938.256
Ξ^0	1314.900
K^0	497.750
Λ	1115.000
π^0	134.975
$\pi^\pm$	139.579

MONTE CARLO PROGRAMS

Program MONTE generated the events to be tested. All beam particles were presumed to travel along the positive x axis and to interact in the target with a k zero and neutral cascade emerging and subsequently decaying. The kinematic values for each event were chosen in the following manner:

beam momentum - the momentum values obeyed a Gaussian distribution with a central value of 1800 MeV/c and a standard deviation of 40 MeV/c

point of interaction - these points were distributed uniformly over the area presented by the flask to the beam and uniformly along the length of the flask

cascade production angles - the center of mass polar angle with respect to the beam direction was chosen according to a $\cos^2$ distribution while the azimuthal angle, as were all such angles, was chosen from a uniform distribution

cascade and k decay points - the known lifetimes were used in conjunction with an exponential decay distribution.

Using similary techniques for other quantities, momentum conservation, and Lorentz transformations, the directions of the four final state charged particles were determined and recorded on tape.

The next step in handling these events was to see whether or

not they would result in a good event signal. Program CARLO followed the particle tracks to see if the anticoincidence counter was triggered and if the hodoscope counted four particles. If the event was detected, the spark locations in the chambers were determined. Each gap had an 80% chance of firing. For those events in which all tracks had more than two visible sparks, a ray was traced through the virtual camera to the film. The film coordinates were randomly varied to simulate measuring errors and then written on tape. The output of CARLO was identical in format to that of the SCAMP measuring system. This allowed the Monte Carlo events to be reconstructed in exactly the same manner as the real data.